

UC San Diego

UC San Diego Electronic Theses and Dissertations

Title

Conducting polymer nanostructures for biological applications

Permalink

<https://escholarship.org/uc/item/5d89v1h1>

Author

Berdichevsky, Yevgeny

Publication Date

2006

Peer reviewed|Thesis/dissertation

UNIVERSITY OF CALIFORNIA, SAN DIEGO

Conducting Polymer Nanostructures for Biological Applications

A dissertation submitted in partial satisfaction of the

requirements for the degree Doctor of Philosophy

in

Electrical Engineering (Electronic Circuits and Systems)

by

Yevgeny Berdichevsky

Committee in charge:

Professor Yu-Hwa Lo, Chair

Professor Sadik Esener

Professor Mike Heller

Professor Sung-Ho Jin

Professor Deli Wang

2006

Copyright©

Yevgeny Berdichevsky, 2006

All rights reserved

The dissertation of Yevgeny Berdichevsky is approved, and it is
acceptable in quality and form for publication on microfilm:

Chair

University of California, San Diego

2006

TABLE OF CONTENTS

Signature Page.....	iii
Table of Contents.....	iv
List of Symbols and Abbreviations.....	vi
List of Figures and Tables.....	vii
Acknowledgements.....	x
Vita and Publications.....	xii
Abstract of the Dissertation.....	xviii
CHAPTER ONE.....	1
Introduction	
CHAPTER TWO.....	5
Polypyrrole Artificial Muscles – Synthesis and Actuation	
2.1 Introduction.....	6
2.2 Polypyrrole Electrochemistry.....	6
2.3 Actuation of Polypyrrole Microstructures.....	16
2.4 Integration of Polypyrrole Microstructures with Silicon Devices.....	23
2.5 Acknowledgments.....	25
2.6 References.....	26
CHAPTER THREE.....	27
Polymer Microvalve Based on Anisotropic Expansion of Polypyrrole	
3.1 Abstract.....	28
3.1 Introduction.....	28
3.2 Concept.....	30
3.3 Experiment.....	32
3.4 Results.....	37
3.5 Conclusion.....	39
3.6 Acknowledgements.....	39

3.7 References.....	40
CHAPTER FOUR.....	41
Fabrication of Polypyrrole Nanowires	
4.1 Abstract.....	42
4.2 Introduction.....	42
4.3 Experiment and Discussion.....	43
4.4 Conclusion.....	53
4.5 Acknowledgements.....	54
4.6 References.....	54
CHAPTER FIVE.....	56
Polypyrrole Nanowire Actuators	
5.1 Introduction.....	57
5.2 Polypyrrole Nanowire Electropolymerization and Evaluation of the Electrochemically Controlled Volume Change.....	59
5.3 Polypyrrole Nanowire Morphology.....	67
5.4 Time Response of Isolated Nanowires.....	71
5.5 Conclusion.....	79
5.6 Appendix.....	79
5.7 Acknowledgments.....	80
5.8 References.....	81
CHAPTER SIX.....	83
Template-fabricated Nanoscale Biosensors for Catecholamine Detection	
6.1 Introduction	84
6.2 Experiment.....	85
6.3 Discussion.....	89
6.4 Conclusion.....	91
6.5 Acknowledgments.....	92
6.6 References.....	92
APPENDIX.....	93
Experimental Details of Nanowire Fabrication and SEM Images	

LIST OF SYMBOLS AND ABBREVIATIONS

PPy: polypyrrole

DBS: dodecylbenzenesulfonate

PDMS: polydimethylsiloxane

UV: ultraviolet

XRD: x-ray diffraction

SEM: Scanning Electron Microscopy

LIST OF FIGURES AND TABLES

Chapter Two Figures

Figure 2.1	Experimental setup	7
Figure 2.2	Polypyrrole chemical structure	9
Figure 2.3	Chemical structure of NaDBS	10
Figure 2.4	Cyclic voltammogram of PPy(DBS)	11
Figure 2.5	Schematic cross-section of a polypyrrole film	13
Figure 2.6	Chronoamperogram of a large area polypyrrole film	14
Figure 2.7	Steps for the microfabrication of polypyrrole test lines	17
Figure 2.8	Optical micrographs of polypyrrole test lines	19
Figure 2.9	Experimental setup for measurement of volume change	20
Figure 2.10	Polypyrrole thickness change with applied voltage	21
Figure 2.11	Operation of PPy Microactuator Integrated with Si Photodiode	24
Figure 2.12	Modulation of PPy expansion/contraction with incident light	25

Chapter Three Figures

Figure 3.1	Proposed Microvalve	31
Figure 3.2	Forces exerted by expanding polypyrrole on 2D and 3D electrodes	32
Figure 3.3	Microfabrication process for polypyrrole actuator	33
Figure 3.4	Micrograph of the cross-section of working microfluidic channel	35
Figure 3.5	Micrograph of the top view of microvalve	36

Figure 3.6 Top view of closed and open microvalves	38
--	----

Chapter Four Figures

Figure 4.1 Polypyrrole nanowire template synthesis	44
Figure 4.2 Top and side views of the polypyrrole nanowires	46
Figure 4.3 Cyclic voltammogram of PPy(DBS) nanowires	47
Figure 4.4 Schematic of nanowire spanning the gap between gold lines	48
Figure 4.5 Cross-sections of alumina anodized on planar substrates	52
Figure 4.6 Gold-polypyrrole heterostructure nanowires	53

Chapter Five Figures

Figure 5.1 SEM top view of PPy(DBS) nanowires, before and after mechanical lapping	60
Figure 5.2 Schematic representation of the nanowire actuator process flow	61
Figure 5.3 SEM images of the alumina surface with embedded nanoactuators	62
Figure 5.4 Nanowire macro- bimorph actuation	64
Figure 5.5 Expansion of polypyrrole nanowires and nanowire cyclic voltammetry ..	65
Figure 5.6 XRD data for PPy (DBS) film and nanowires	69
Figure 5.7 Fabrication sequence for electropolymerization of isolated PPy nanowires	72
Figure 5.8 SEM images of isolated PPy(DBS) nanowire groups	73
Figure 5.9 Chronoamperogram and cyclic voltammogram of isolated PPy nanowires	74
Figure 5.10 Concentration profile versus distance at various times.....	77
Figure 5.11 Diffusion-controlled current plotted versus dimensionless time.....	78

Chapter Six Figures

Figure 6.1 Fabrication sequence for Au nanoelectrodes	86
Figure 6.2 SEM images at different stages of the fabrication	87
Figure 6.3 Current response due to addition of small concentrations of dopamine ...	89
Figure 6.4 Differential pulse stripping voltammetry	91

Appendix Figures

Figure A.1 Alumina membrane with 200 nm pore diameter.....	95
Figure A.2 Polystyrene microbeads on alumina surface.....	96
Figure A.3 Sputtering of 300 nm SiO ₂ film onto alumina/bead substrate.....	97
Figure A.4 Alumina membrane with 20 nm pore diameter.....	98

Chapter Four Table

Table 4.1	Resistance Measurements of PPy Nanowires	49
-----------	--	----

ACKNOWLEDGEMENTS

I would like to thank my advisor, Yu-Hwa Lo, for his support and encouragement throughout my graduate work, and the staff of Integrated Technologies Laboratory (ITL) for their valuable technical support. I would also like to thank Eileen Kennedy and my parents, Lisa and Yuriy Berdichevsky, for their unconditional support, help, and for always believing in me.

The work in this dissertation was funded by the AFOSR MURI program.

The text of Chapter 2 is, in part, a reprint of the material as it appears in Y. Berdichevsky, Y.-H. Lo, *Lasers and Electro-Optics Society, The 17th Annual Meeting of the IEEE*, Vol. 2, 507-508, 2004. The dissertation author was the primary researcher and author and the co-author listed in this publication directed and supervised the research which forms the basis of this chapter.

The text of Chapter 3 is, in part, a reprint of the material as it appears in Y. Berdichevsky, Y.-H. Lo, *Mat. Res. Soc. Symp. Proc.* Vol. 782, A4.4.1-A4.4.7, 2004. The dissertation author was the primary researcher and author and the co-author listed in this publication directed and supervised the research which forms the basis of this chapter.

The text of Chapter 4 is, in part, a reprint of the material as it appears in Y. Berdichevsky, Y.-H. Lo, *Smart Structures and Materials 2005: Electroactive Polymer*

Actuators and Devices, Proc. SPIE Vol. 5759, 268-273, 2005. The dissertation author was the primary researcher and author and the co-author listed in this publication directed and supervised the research which forms the basis of this chapter.

The text of Chapter 5 is, in part, a reprint of the material as it appears in Y. Berdichevsky, Y.-H. Lo, *Mater. Res. Soc. Symp. Proc.* Vol. 872, J13.4.1-J13.4.5, 2005, and *Advanced Materials* 18, 122-125, 2006. The dissertation author was the primary researcher and author and the co-author listed in these publications directed and supervised the research which forms the basis of this chapter.

VITA AND PUBLICATIONS

EDUCATION

B.S. Engineering (Electrical Engineering and Computer Science) June 1999

University of California, Berkeley

M.S. Electrical and Computer Engineering October 2002

University of California, San Diego

Advisor: Yu-Hwa Lo

Ph.D. Electrical Engineering (Electronic Circuits and Systems) June 2006

University of California, San Diego

Advisor: Yu-Hwa Lo

Dissertation: “Conducting Polymer Nanostructures for Biomedical Applications”

EXPERIENCE

Graduate Student 2000-2006

University of California, San Diego

Designed, fabricated, and evaluated conducting polymer microstructures and nanowires for use as actuators in micro- and nanofluidic systems and biomedical devices. Evaluated nanowire electrochemical properties in biologically relevant

electrolyte, and reported first evidence of electrically controlled nanowire actuation detected with optical and scanning electron microscopy.

Designed and fabricated polymer (PDMS) microfluidic devices, modified surface properties of PDMS for improved device performance, and designed integrated conducting polymer microvalve and microoptical components in microfluidic devices for DNA electrophoresis and cell cytometry.

Teaching Assistant

Electromagnetism lecture course for junior and senior undergraduate students 2006

Microstructure Processing Technology Lab Course for junior and senior undergraduate students. 2005

Engineering Consultant 2000-2001

Torrey Mesa Research Institute, La Jolla, CA

DNA electrophoresis in PDMS microfluidic chips, design and implementation of customized high voltage power supply for biomolecule separations, engineering service for thin-gel DNA electrophoresis system.

Engineer 1999-2000

LSI Logic Corporation, Milpitas, CA

Implementation and evaluation of datapath design methodology for synthesis and layout of VLSI chips; CAD algorithm implementation, design of digital timing circuits.

AWARDS

MICRO Fellowship, University of California	2000-2001
LSI Logic Corp. Invention Award	2000

MEMBERSHIP

Institute of Electrical and Electronics Engineers (IEEE)	1997-present
--	--------------

JOURNAL PUBLICATIONS

1. **Y. Berdichevsky** and Y.-H. Lo, “Effects of Template Synthesis on Polypyrrole-dodecylbenzenesulfonate Nanowire Morphology and Time Response,” in preparation.
2. **Y. Berdichevsky** and Y.-H. Lo, “Template-fabricated nanoscale biosensors for catecholamine detection,” in preparation.
3. **Y. Berdichevsky** and Y.-H. Lo, “Polypyrrole Nanowire Actuators,” *Advanced Materials* 18, 122-125, 2006.
4. **Y. Berdichevsky**, J. Khandurina, A. Guttman and Y.-H. Lo, “UV/ozone Modification of Poly(dimethylsiloxane) Microfluidic Channels,” *Sensors and Actuators B* 97, 402-408, 2004.
5. V. Lien, K. Zhao, **Y. Berdichevsky** and Yu-Hwa Lo, “High-Sensitivity Cytometric Detection Using Fluidic-Photonic Integrated Circuits with Array Waveguides,” *IEEE Journal of Selected Topics in Quantum Electronics* 11(4), 827-834, 2005.
6. V. Lien, **Y. Berdichevsky** and Y.-H. Lo, “A Prealigned Process of Integrating Optical Waveguides with Microfluidic Devices,” *Photonics Technology Letters* 16(6), 1525 – 1527, 2004.
7. D.-Y. Zhang, N. Justis, V. Lien, **Y. Berdichevsky** and Y.-H. Lo, “High-Performance Fluidic Adaptive Lenses,” *Applied Optics*, 2004.
8. V. Lien, **Y. Berdichevsky** and Y.-H. Lo, “Microspherical Surfaces with Predefined Focal Lengths Fabricated Using Microfluidic Capillaries,” *Applied Physics Letters*, 83, 5563, 2003.

9. V. Lien, Y. Wu, D. Zhang, **Y. Berdichevsky**, J. Choi and Y.-H. Lo, “A Novel Technology for Fabricating Gratings of Any Chirp Characteristics by Design,” *Photonics Technology Letters*, 15(5), 712 – 714, 2003.
10. D.-Y. Zhang, V. Lien, **Y. Berdichevsky**, J. Choi and Y.-H. Lo, “Fluidic Adaptive Lens with High Focal Length Tunability,” *Applied Physics Letters*, 82, 3171, 2003.

PODIUM PRESENTATIONS AND CONFERENCE PUBLICATIONS

1. **Y. Berdichevsky**, “Polymer Nanostructure Actuation in Aqueous Environment,” *UCSD Electronic Materials and Devices Research Seminar*, 2005, invited.
2. **Y. Berdichevsky** and Y.-H. Lo, “Fabrication and Evaluation of Conducting Polymer Nanowire Heterostructures,” *Mater. Res. Soc. Symp. Proc.* Vol. 872, J13.4.1-J13.4.5, 2005.
3. **Y. Berdichevsky** and Y.-H. Lo, “Fabrication of Polypyrrole Nanowires,” *Smart Structures and Materials 2005: Electroactive Polymer Actuators and Devices, Proc. SPIE* Vol. 5759, 268-273, 2005.
4. **Y. Berdichevsky** and Y.-H. Lo, “Integration of conducting polymer micro- and nano-actuators with semiconductor photonic devices,” *Lasers and Electro-Optics Society, The 17th Annual Meeting of the IEEE*, Vol. 2, 507 – 508, 2004.
5. **Y. Berdichevsky** and Y.-H. Lo, “Polymer Microvalve Based on Anisotropic Expansion of Polypyrrole,” *Mat. Res. Soc. Symp. Proc.* Vol. 782, A4.4.1-A4.4.7, 2004.

6. **Y. Berdichevsky**, J. Khandurina, Y.-H. Lo and A. Guttman, “UV/Ozone Modification of PDMS Microfluidic Devices,” *HPCE 2003*.
7. V. Lien, **Y. Berdichevsky** and Y.-H. Lo, “Fabrication of Concave Micro-mirrors with Programmable Focal Lengths Using Microfluidic Capillary,” *2003 CLEO Conference on Lasers and Electro Optics*, 293-295, 2003.
8. V. Lien, **Y. Berdichevsky** and Y.-H. Lo, “Monolithically Integrating Photonic and Microfluidic Devices Using a Self-aligned Process,” *Lasers and Electro-Optics Society, The 16th Annual Meeting of the IEEE*, Vol. 2, 525 – 526, 2003.
9. V. Lien, **Y. Berdichevsky**, Y.-H. Lo, J. Khandurina and A. Guttman, “Monolithic photonics-microfluidics integration for micrototal analysis systems,” *Lasers and Electro-Optics CLEO '03*.
10. V. Lien, Y. Wu; D. Zhang, **Y. Berdichevsky**, J. Choi and Y.-H. Lo, “A Novel Technology for Fabricating Gratings of Any Chirp Characteristics by Design,” *Lasers and Electro-Optics Society, The 15th Annual Meeting of the IEEE*, Vol. 2, 799 – 800, 2002.

PATENT

US Patent 6611951: **Y. Berdichevsky**, A. Tetelbaum, “Method for estimating cell porosity of hardmacs”, 2003.

ABSTRACT OF THE DISSERTATION

Conducting Polymer Nanostructures for Biological Applications

by

Yevgeny Berdichevsky

Doctor of Philosophy in Electrical Engineering (Electronic Circuits and Systems)

University of California, San Diego, 2006

Professor Yu-Hwa Lo, Chair

A novel polypyrrole nanowire actuator was fabricated and characterized, representing a completely new approach to the design of nanoscale mechanically active components (nanomachines). This design paradigm takes advantage of the fact that unique properties of polypyrrole allow development of mechanically active nanostructures capable of operating in aqueous salt solutions with many potential applications biology and medicine.

Template synthesis technique was used to electropolymerize polypyrrole nanowires in the nanoporous alumina templates. Commercial alumina filters were used both “as is” and patterned with microbeads to reduce the open pore density, along with anodized alumina prepared as a thin film on a semiconductor substrate. The

ability of the nanowires to expand and contract with applied voltage was then evaluated with scanning electron microscopy and high-resolution optical microscopy. It was confirmed that the nanowires can function as nanoactuators, which is a significant advance in developing nanomechanical structures. Polypyrrole nanoactuators are electrically controlled, rather than relying on changing the chemical composition of solution, can be easily synthesized in parallel and in high numbers without requiring e-beam lithography, and can operate in aqueous salt solutions at biologically-relevant pH. Furthermore, the speed of polypyrrole actuators depends on their size due to diffusion limitations, and nanoactuators are therefore able to operate at higher speeds than micro- or macro- sized devices.

The development of these nanoactuators paves the way for mimicking the function of biological actuators such as cilia, creation of controllable membranes, small particle manipulation, cellular nanomechanical probes, and many other biomedical applications. Furthermore, the same technology and process flow used for fabrication of nanoactuators was also used to create nanosensors for detection of electrochemically oxidizable neurotransmitters such as catecholamines. The small size of the sensors allowed rapid time response and detection of low concentrations of dopamine.

CHAPTER 1

Introduction

The conducting polymer polypyrrole possess many interesting properties that make it an attractive material for a variety of applications. In particular, the reversible redox reactions that this polymer undergoes in electrolyte with applied voltage allow control over many material properties such as conductivity, ion exchange, hydrophobicity, and even the material dimensions. The control of ion exchange properties of the polymer is important in the design of selective sensors, while voltage control over material geometry makes polypyrrole particularly suited as a material for design of actuators. Furthermore, the controllable ion exchange and volume change are material properties of polypyrrole, and can be utilized at any dimension ranging from macroscale, or devices several centimeters in size, to nanoscale, or devices with the size of several tens of nanometers. This flexibility allows the design of a great variety of polypyrrole devices, including “artificial muscles” intended for medical prosthetics, microactuators for lab-on-a-chip integrated systems and microrobotics, and sensors for various biological molecules.

In this work, polypyrrole doped with dodecylbenzenesulfonate (DBS) is used to make devices capable of operating in aqueous environments. DBS-doped polypyrrole has long term stability in water solutions, and operates by uptaking or expelling small positive ions during voltage-controlled reduction or oxidation, respectively, from the surrounding electrolyte. This property makes polypyrrole (DBS) devices particularly suited for biomedical applications, where the environment consists of an electrically conducting aqueous solution containing a number of small ions such as Na^+ , K^+ , and Ca^{2+} . Therefore, a polypyrrole actuator device that operates

on the principle of volume change due to the movement of sodium ions can use the biological solution such as extracellular fluid or blood plasma as a supporting electrolyte without the need for device encapsulation.

In this work, several novel devices based on the properties of polypyrrole are described, including a microvalve based on a polypyrrole microactuator, polypyrrole nanowires capable of reversible length change with the applied voltage, and a polypyrrole-coated nanosensor for detection of catecholamine neurotransmitters that displays nanomolar sensitivity and improved time response. The nanowire actuators described in this work represent a breakthrough in the design of artificial actuators that approach the function and performance of natural biological mechanical elements such as the skeletal muscle fibers. Biological actuators are capable of doing mechanical work by changing their length, in aqueous environment, with the time scale of several tens of milliseconds. The artificial nanowire actuators reported here match this performance, and can be used for design of a completely novel class of devices for biomedical applications.

The organization of this work is briefly outlined here: in chapter 2, electrochemical properties of polypyrrole that enable the operation of actuator devices are examined, and the technology for fabrication of polypyrrole microstructures and their integration with semiconductor devices is described. In chapter 3, the design of a polydimethylsiloxane (PDMS) microvalve that uses a polypyrrole actuator as a mechanically active element is presented. The template synthesis technology for fabrication of polypyrrole nanowires is shown in chapter 4, while the evaluation of

nanowires as nanoactuators with optical and electron microscopy, electrochemical techniques, and x-ray diffraction is described in chapter 5. Finally, in chapter 6, the technology used for fabrication of dispersed polypyrrole nanowires is adopted to make nanosensors for neurotransmitter detection with nanomolar precision and rapid time response.

CHAPTER 2

Polypyrrole Artificial Muscles – Synthesis and Actuation

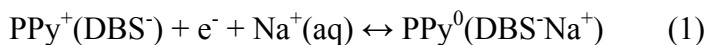
2.1 INTRODUCTION

Conducting polymer actuators are well suited for applications in biological and medical microsystems [1]. These actuators can change their volume due to an electrochemically induced redox reaction, with attendant movement of ion and solvent in and out of the polymer matrix. The resulting volume change can be as large as 30% with applied voltage of only a few volts [2]. Low voltage requirements, large relative displacement, and ability to operate in aqueous environments make conducting polymer actuators promising candidates for microfluidics [3], micromachined biological sensors, and lab-on-chip devices for manipulation of cells and organelles. Of further interest is the ability to microfabricate conducting polymer structures on semiconductor substrates, leading to intriguing possibilities of integrating actuator functionality with optical modulation or optical power transfer. Furthermore, conducting polymer nanostructures can also be fabricated, with suggested applications in areas such as biosensors, bioencapsulation, and drug delivery [4].

2.2 POLYPYRROLE ELECTROCHEMISTRY

Polypyrrole is one of the conducting polymers which have been used as actuators, or “artificial muscles”. Polypyrrole (PPy) can be fabricated by electrochemical synthesis on a conducting substrate [5]. In this work, polypyrrole doped with DBS⁻ (dodecylbenzenesulfonate) anions was used. When voltage is

applied to this polymer in an aqueous solution containing a small positive ion, such as Na^+ , the PPy undergoes a redox reaction:



Insertion of Na^+ and its hydration shell causes swelling of polymer matrix, while expulsion of Na^+ ions results in shrinking. Reliance on a ubiquitous small positive ion such as Na^+ allows PPy to function in a variety of aqueous environments such as blood, urine, cell culture media, and even sea water.

2.2.1 Electropolymerization of Polypyrrole Polypyrrole can be polymerized by either purely chemical or electrochemical means by oxidizing the monomer, pyrrole. In this work, aqueous electrochemical synthesis was used. The experimental setup is shown schematically in Figure 2.1.

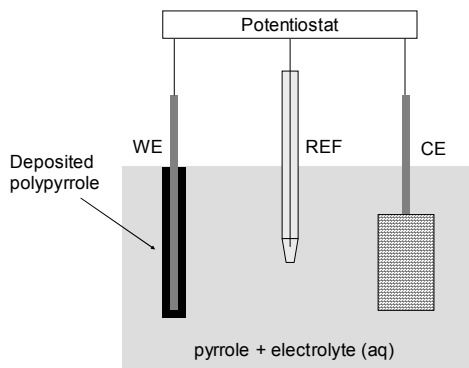


Figure 2.1. Experimental setup. WE: working electrode; REF: reference electrode, CE: counter electrode, deposited polypyrrole is shown in black covering the working electrode.

A three electrode electrochemical system was used, including the working electrode on which polypyrrole was synthesized, an Ag/AgCl reference electrode, and a

platinum mesh counter electrode. The potentiostat (Gamry Instruments) maintains a defined voltage between the working and reference electrodes while passing the current between working and counter electrodes. This arrangement has the benefit of allowing a well defined voltage to be set at the working electrode while isolating the any voltage drop that can occur at the counter electrode. The solution used for polypyrrole synthesis was 0.1 M pyrrole monomer dissolved in 0.1 M NaDBS aqueous electrolyte. NaDBS solution was made in large quantities with deionized water and used as needed in the experiments. Pyrrole (Sigma-Aldrich) was stored in a septum-covered bottle under nitrogen atmosphere in a -4°C freezer prior to the experiments to avoid spontaneous oxidation, and was added to the solution a short time before the start of the experiment. Polypyrrole was synthesized by maintaining a 0.55V difference between the working electrode and an Ag/AgCl reference. This voltage is anodic enough to oxidize pyrrole monomers in contact with the working electrode by removing electrons from the molecules, which then dimerize, trimerize, and eventually polymerize into polypyrrole chains. These chains then precipitate out of the solution onto the working electrode surface. The thickness of the deposited polypyrrole is controlled by the time of the deposition; for large area WE ($> 1\text{ cm}^2$), the deposition rate is approximately $1\text{ }\mu\text{m/hr}$. Films as thick as $40\text{ }\mu\text{m}$ can be deposited with this method. The color of the deposited films changes depending on the thickness for films thinner than $1\text{ }\mu\text{m}$, for thicker films the color is black. Smooth glossy films with thicknesses up to $10\text{ }\mu\text{m}$ can be produced, however, the roughness of the film surface tends to increase with increased thickness.

2.2.2 Polypyrrole Conductivity. Polypyrrole is considered a conducting polymer due to its conjugated backbone (Figure 2.2).

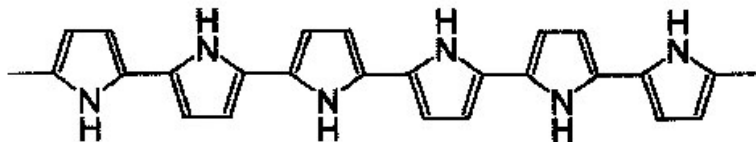


Figure 2.2 Polypyrrole chemical structure

The electrons shown schematically as the double bonds in the chemical structure of polypyrrole are mobile and can move from one pyrrole unit to the other on the chain. If there are defects in the synthesized polypyrrole, or if there are intentionally introduced dopant ions, such as the DBS⁻ ion in this work, the double bonds can become ionized (electrons removed or added), to form structures known as solitons, polarons, and bipolarons. In polypyrrole, the conduction mechanism is “bipolaron hopping” along the polymer chain. In a heavily doped polymer, the presence of many bipolarons generates bipolaron conduction bands in the material bandgap, and the polymer becomes conductive. In the case of polypyrrole doped with dodecylbenzenesulfonate, the conductivity is on the order of $10 (\Omega \cdot \text{cm})^{-1}$, depending on the oxidation state and the temperature [6].

2.2.3 Doping of Polypyrrole with DBS ions. The presence of sodium dodecylbenzenesulfonate in the synthesis solution serves several functions: first, NaDBS functions as a conducting electrolyte to allow oxidation of pyrrole monomers, second, NaDBS is an amphiphilic surfactant that allows a high concentration of hydrophobic pyrrole monomer to be dissolved in an aqueous solution, and third, and

most important, the DBS⁻ ion becomes incorporated into the polymer matrix during synthesis and serves as a dopant ion. Dodecylbenzenesulfonate is a large molecule with a long hydrophobic tail (Figure 2.3)

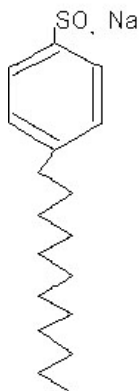


Figure 2.3 Chemical structure of sodium dodecylbenzenesulfonate (NaDBS)

Due to its size and the favorable hydrophobic-hydrophobic interactions with the polypyrrole, dodecylbenzenesulfonate ions become permanently imbedded in the polymer matrix, acting as a permanent dopant and also altering the polymer nanostructure, as will be discussed in Chapter 4. The degree of the doping is far higher in polypyrrole than the typical doping in inorganic semiconductors; in polypyrrole, there is roughly one DBS ion per 4 pyrrole units.

2.2.4 Electrochemical Cycling of PPy(DBS). For electrochemical testing of polypyrrole doped with dodecylbenzenesulfonate ions, the experimental setup shown in Figure 2.1 was used, with a NaDBS aqueous electrolyte (with no pyrrole monomers). The voltage range versus the Ag/AgCl reference was 0 to -1 V, corresponding to approximately 0 to -2.5 V measured between working and counter electrodes. Polypyrrole is electrochemically reduced at -1 V, and oxidized at 0 V. In

equation (1), the left side, $\text{PPy}^+(\text{DBS}^-)$, represents the polymer in its oxidized state, while the right side, $\text{PPy}^0(\text{DBS}^-)\text{Na}^+$, represents the reduced polymer. As the application of negative voltage adds electrons to the polymer backbone (reduction), charge neutrality has to be preserved, and the sodium ions move in from the surrounding electrolyte into the polymer matrix to compensate for the negative charge on the immobile DBS^- dopant ions. When oxidizing voltage is applied to the polymer (0 V vs. Ag/AgCl), electrons are removed from polypyrrole, resulting in a positively charged polymer matrix that pushes mobile sodium ions out to the surrounding solution to preserve charge neutrality. The reaction is reversible, and can be carried out by applying a voltage ramp to the polymer while measuring the oxidizing/reducing currents, as shown in Figure 2.4.

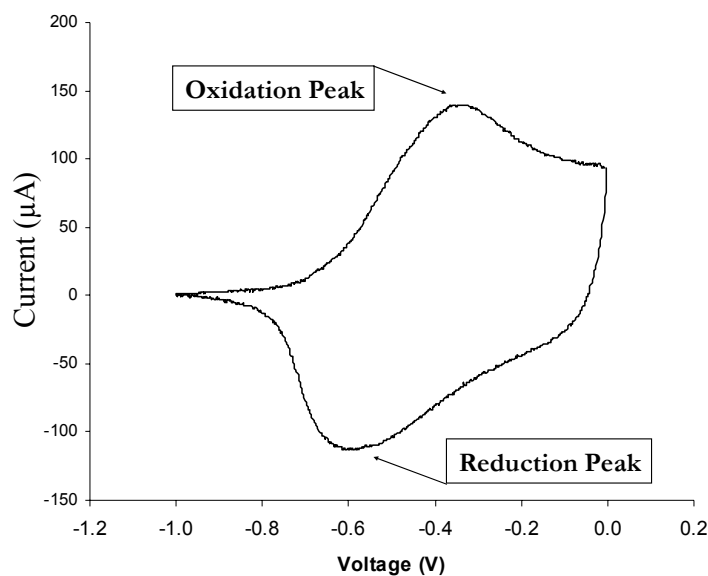


Figure 2.4 Cyclic voltammogram of PPy(DBS) in 0.1 M NaDBS electrolyte at 50 mV/sec voltage scan

This electrochemical method is known as cyclic voltammogram, and it allows determination of the voltages at which oxidation and reduction reactions take place. Tracing the voltammogram from 0 V through the reduction peak to -1 V and back through oxidation peak to 0 V, the following events take place: the polymer starts out in the oxidized state, and as the voltage is lowered, the potential barrier for adding electrons onto the polymer backbone is overcome, and the current due to polymer reduction begins to flow. The reduction current reaches its peak at -0.6 V and begins to taper off as the polymer matrix becomes fully reduced. This is accompanied by simultaneous movement of Na^+ ions from the electrolyte into the polymer to compensate the negative charge on DBS^- dopant ions. At -1 V, the current has reached its minimum, signifying that the reduction of the polymer is complete. If the voltage was lowered further, the current would begin to increase again due to water electrolysis which would damage the polymer. Therefore, the applied voltage is limited to -1 V, as this is low enough to reduce the polymer without negative effects of electrolysis. As the voltage is then increased on the return scan, oxidation current can be observed due to the electrons being removed from the polymer and the corresponding movement of Na^+ ions out of the PPy matrix. The peak occurs at -0.35 V, and the current reaches a minimum at 0 V, corresponding to a complete oxidation of the polypyrrole. At higher voltages, an irreversible oxidation of the polymer occurs, accompanied by chemical changes to the polypyrrole structure. If allowed, this would render polypyrrole unusable; therefore, the applied oxidation voltage is limited to 0 V.

2.2.5 Volume Change Due to Reversible Electrochemical Redox Reaction

of PPy(DBS). As the polymer is electrochemically cycled between 0 and -1 V, movement of Na^+ in and out of the polypyrrole matrix occurs as described above. Each Na^+ ion is accompanied by a solvation shell of several water molecules, and, in addition, osmotic pressure causes a more water molecules to enter the polymer alongside the sodium ions [7]. The additional volume of Na^+ ions and water that have entered the polypyrrole film cause conformational changes of the polypyrrole molecules and changes in the overall dimensions of the deposited polypyrrole (Figure 2.5).

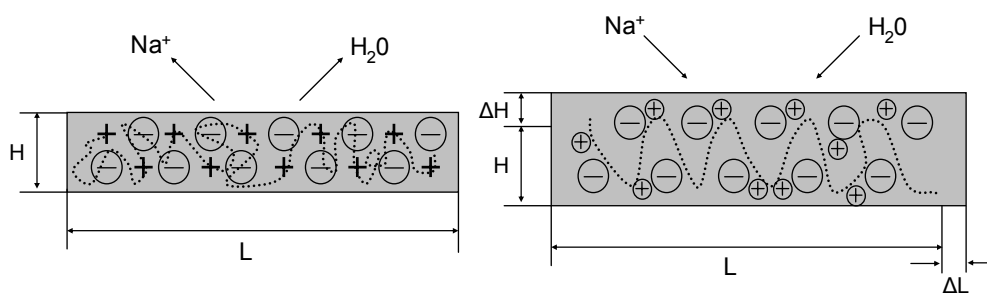


Figure 2.5. Schematic cross-section of a polypyrrole film. Oxidized film ($V_{\text{vs Ag/AgCl}} = 0 \text{ V}$) is shown on the left, with sodium ions and water expelled from the polymer matrix, polymer backbone charged positive (+ signs), compensating the charge on immobile DBS^- ions (encircled (-) signs). Reduced film is on the right, with the neutral polymer backbone, and Na^+ ions entering the film (encircled (+) signs) to compensate the charge on DBS^- ions.

As can be seen in the figure, the applied voltage and entering sodium ions and water molecules cause a conformation change of the polypyrrole chains (black dotted lines), with the resulting volume change of the film. If the film has length L and thickness H , the expansion of the film under reducing voltage can be as high as $\Delta L/L = 2\text{-}3\%$ and $\Delta H/H = 30\%$. The increase in length is used in so-called “bilayer actuators”, where a polypyrrole film is laminated to a thin film of another material that doesn’t undergo

volume changes with applied voltage – this allows the magnification of the relatively small changes in the length of PPy film and results in large scale movement. The reversible increase in thickness, on the other hand, is relatively large compared to the size of the synthesized film, and can be used directly in micro- and nano- actuators discussed in this work.

2.2.6 Time Response of the Polypyrrole Films. A polypyrrole film chronoamperogram, or current response to applied voltage steps plotted versus time, is shown in Figure 2.6.

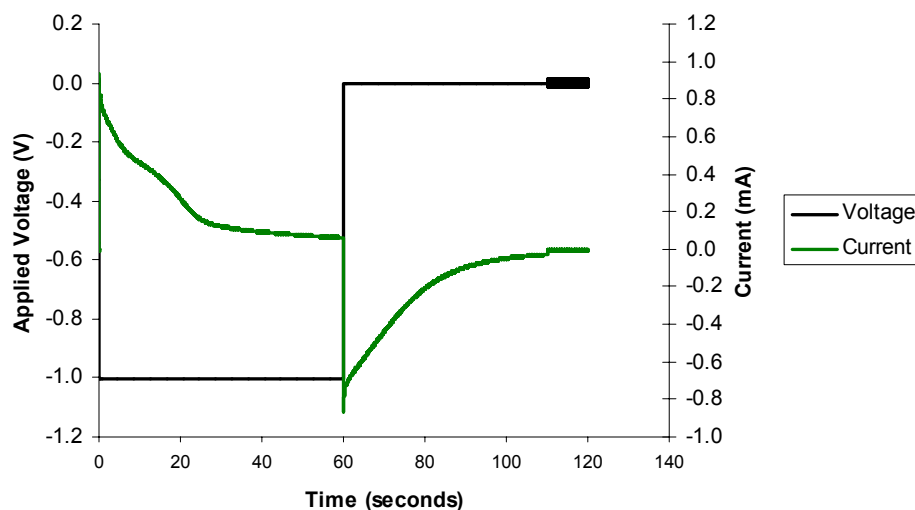


Figure 2.6 Chronoamperogram of a large area ($> 1 \text{ cm}^2$) $30 \text{ }\mu\text{m}$ thick polypyrrole film.

The experimental setup used to perform chronoamperometry is the same as the one described above for cyclic voltammetry. A defined voltage is applied between the working and reference electrodes, while current is measured between working and counter electrodes. Working electrode is kept at 0 V prior to the start of the experiment, reducing voltage of -1 V versus Ag/AgCl is applied at $t = 0$ seconds, and

an oxidizing voltage of 0 V versus Ag/AgCl is applied at $t = 60$ seconds. In Figure 2.6, the current response to the voltage steps can be observed: first, there is a large current spike that corresponds to charging of the double layer capacitance, and then the current begins to decay as the polymer becomes reduced or oxidized and ions diffuse in and out of the polymer matrix, respectively. The time response of the current is not due purely to ion diffusion, however. An inflection point can be seen clearly in the reducing current, and the oxidizing current is not a simple exponential decay that could be expected as the remaining ions leave the polymer by diffusion. The change in conformation of polypyrrole chains which occurs both during reduction and oxidation introduces further time delay into the course of the current response [8]. In the oxidized polypyrrole, polymer chains are in a “compacted” conformation, packed close together as there is neither water nor sodium ions in the polymer matrix. When a reducing voltage is applied, the chains take some time to rearrange their conformation state, likely driven by electrostatic repulsion of the dopant DBS⁻ ions whose negative charge is no longer being compensated by the positive charge on the polymer. As the polypyrrole chains move further apart, the structure of the film becomes less dense, allowing ion and water diffusion into the polymer. The current time response is therefore a summation of these two processes, the conformational changes of the polypyrrole chains in response to applied voltage, and the diffusion of sodium ions and water molecules to maintain charge neutrality. The two processes combine to produce the inflection in the measured current at the point where the film

structure becomes fully open and ion diffusion takes over as the current-limiting factor.

A more quantitative analysis of the polypyrrole electrochemical time response is impeded and complicated by the presence of other processes that take place during the reversible redox reaction: changes in conductivity of the polypyrrole film as it passes from an oxidized to a reduced state, current due to capacitive charging of the double layer throughout the polymer (which can be viewed as a conductive porous electrode), the contribution of electric field-driven ion migration [9] to the apparent diffusion constants of Na^+ ions and their water solvation shells, and the uncompensated solution resistance between the electrodes in the electrochemical cell which can introduce a significant voltage drop and effectively lower the applied voltage at the film-solution interface. In Chapter 5, a theoretical analysis of the diffusion contribution to the time course of polypyrrole doping/undoping is presented, and the role of polypyrrole device geometry (shape and size) is examined.

2.3 ACTUATION OF POLYPYRROLE MICROSTRUCTURES

2.3.1 Microfabrication of the Polypyrrole Test Lines. In order to evaluate the ability of polypyrrole microstructures to function as actuators due to electrochemically induced thickness changes, polypyrrole micro test lines of varying width were fabricated using photolithographic techniques and tested in solution using a profilometer and an optical microscope. Microfabrication described here and in later

chapters was performed in the Integrated Technologies Laboratory (ITL) in the Electrical and Computer Engineering (ECE) Department at University of California, San Diego. The fabrication sequence is shown schematically in Figure 2.7. A glass slide or a cover slip are cleaned by ultrasonication, then in a sequence of solvent baths: acetone, isopropanol, methanol, and water, and dried by compressed nitrogen. A thin film of Ti/Au is then sputtered

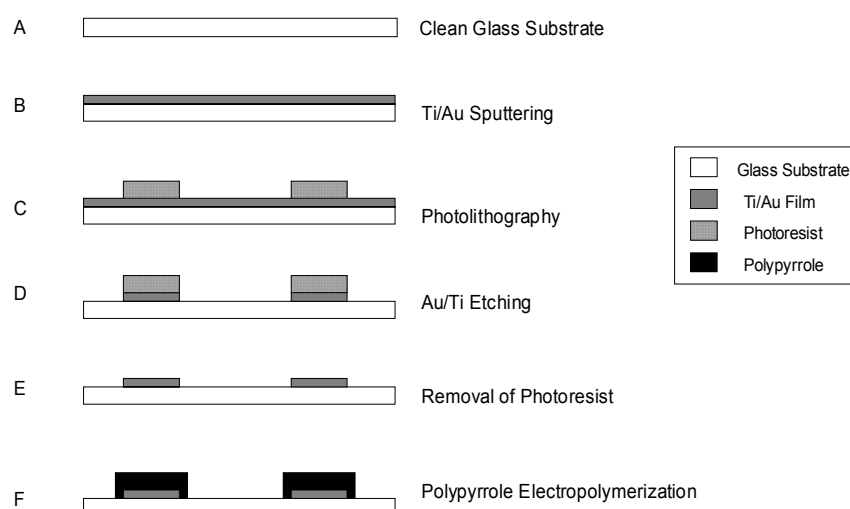


Figure 2.7 Steps for the microfabrication of polypyrrole test lines

on the glass substrate in the Denton Sputtering System. Ti film is used as an adhesion layer between Au film, which acts as a conductive seed layer for polypyrrole deposition later in the process, and glass. Ti and Au are deposited by using Ar plasma sputtering from two metal targets in sequence without exposing the sample to air, to avoid oxidation of Ti and subsequent loss of adhesion between Ti and Au. The sputtering conditions were as follows: 35 sccm Ar flow for used for both metals, with

Ti sputtered at 200 W plasma power for 30 seconds, resulting in a film of approximately 30 nm thickness, and Au sputtered at 400 W for 100 sec to deposit a 200 nm film. In step C in the fabrication sequence, the sample was spin-coated with photoresist and exposed to UV radiation through a chrome-patterned mask in a mask aligner. Both positive S1818 (Shipley) and negative SU8 (Microchem) photoresists were used with dark and light-field masks, depending on the desired pattern, in HTG and Quintel Mask Aligners, depending on the mask size. The photoresists were spun-coated, baked, exposed, and developed according to manufacturers' specifications. OmniCoat layer was spun onto the substrate, as specified by the manufacturer, prior to application of SU8 series photoresists to enable lift-off of the SU8 epoxy after completion of lithography. After the photoresist was developed, the gold layer was dissolved in the exposed areas by commercial Au etch, while in-house prepared SC1 solution (1:1:5 solution of 25% $\text{NH}_3\text{H}_2\text{O}$, 30% H_2O_2 , and DI H_2O) was used to etch the Ti adhesion layer. After completion of the metal etch, photoresist was removed (S1818 in acetone, SU8 by lift-off in Remover PG), and the substrate with the metal line pattern was cleaned further in oxygen plasma (100 W, 2 minutes) to remove any photoresist residues in step E of the fabrication sequence. In the final step, the sample was used as the working electrode in the electrochemical cell for electropolymerization of polypyrrole shown in Figure 2.1. Voltage (0.55 V vs. Ag/AgCl) was applied to all Au/Ti lines simultaneously for 7 hours to produce a film of 6.5 – 7 μm thickness coating the metal (Figure 2.8). Since polypyrrole growth occurs isotropically, a widening of the Au/Ti patterns occurred. The thickness was

uniform over the metal except the edges, where the polypyrrole coating was thicker by approximately $1\text{ }\mu\text{m}$ than in the middle of the metal strip line. This is caused by

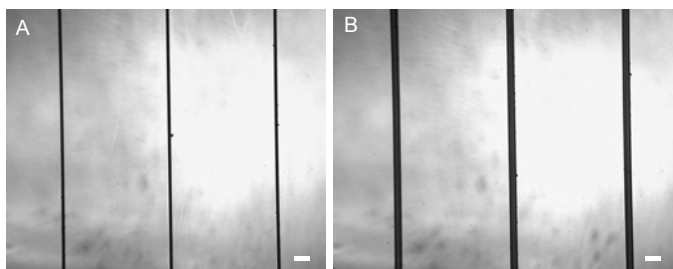


Figure 2.8 Optical micrographs of polypyrrole test lines: A, $5\text{ }\mu\text{m}$ wide PPy lines;; B, $25\text{ }\mu\text{m}$ PPy lines. The scale bars in both images represent a distance of $50\text{ }\mu\text{m}$.

nonuniformity in the electric field and the improved pyrrole monomer diffusion at the edges of the metal lines which act as working electrodes.

2.3.2 Measurement of electrochemically controlled thickness change of polypyrrole test lines. Experimental setup for evaluation of electrochemically induced thickness changes in the polypyrrole test lines is shown schematically in Figure 2.9.

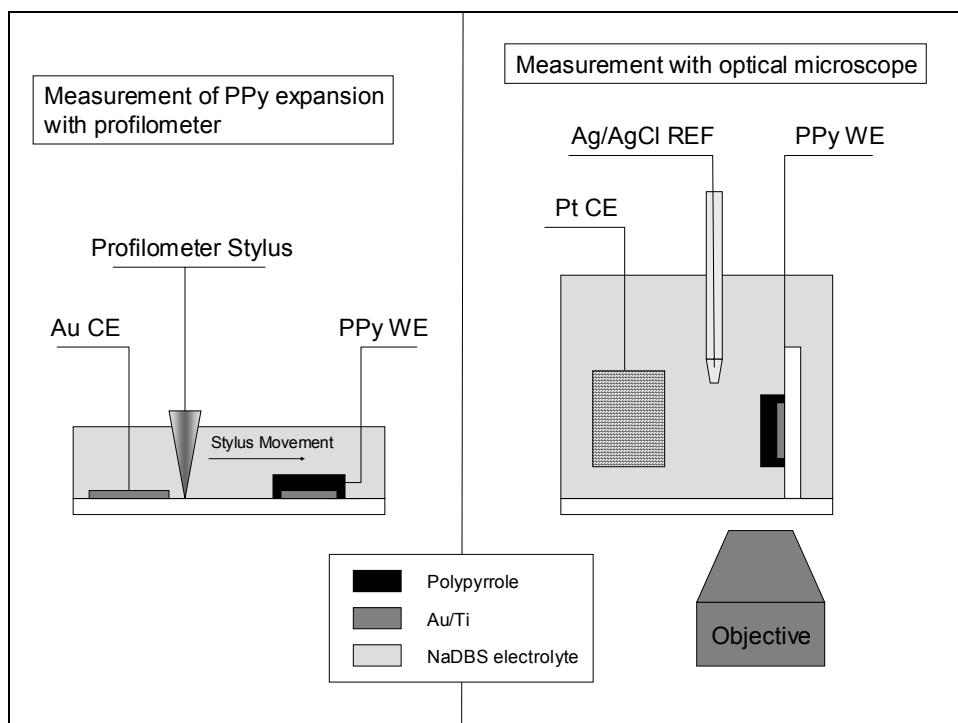


Figure 2.9 Experimental setup for measurement of the electrochemically controlled volume change of polypyrrole test structures. On the left, the profilometer is used to measure the change in thickness of polypyrrole electropolymerized on an Au/Ti line. On the right, an inverted optical microscope images the polypyrrole test line from the side, allowing measurement of the thickness change. WE: working electrode, CE: counter electrode, REF: reference electrode.

Two methods were used to evaluate the thickness changes of the polypyrrole test lines induced by applied voltage: a mechanical profilometer (Dektak) measurement, and optical imaging with a microscope (Nikon TE). The profilometer has the advantage of higher sensitivity and precision, but due to the physical constraints of the equipment used, a very shallow electrolyte bath was used. A gold counter electrode had to be fabricated on the same substrate as the working electrode, while the reference electrode was excluded. Therefore, the voltage was applied between working and counter electrodes, with the same values as were measured between WE and CE in the 3 electrode setup (0 V for oxidizing voltage, -2.5 V for the reducing voltage). The

inverted optical microscope allowed the use of a larger volume electrolyte bath with three electrodes; however, the resolution of this imaging was lower than that of the profilometer. This was due to the relatively long distance between the objective and the measured polypyrrole line, limiting the imaging to lower power or long working distance objectives. Nevertheless, optical imaging has the added advantage of allowing video microscopy with easy visualization of the time course of polypyrrole thickness change. A slightly modified version of the optical microscopy setup was also used to measure the actuation of polypyrrole nanowires, as described in Chapter 5.

The change of polypyrrole line thickness with voltage applied between polypyrrole working electrode and gold counter electrode, measured with profilometry and confirmed with optical microscopy, is shown in Figure 2.10.

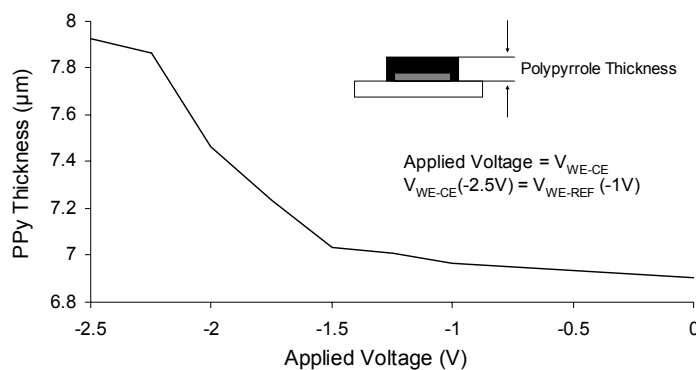


Figure 2.10 Polypyrrole thickness change with applied voltage, measured by profilometry.

As described above, the voltage is applied between polypyrrole working electrode and gold counter electrode; a voltage of -2.5 V between WE and CE is equivalent to $V = -1V$ vs. Ag/AgCl. The measurement shown in Figure 2.10 is taken after the

polypyrrole has been electrochemically cycled a few times. This is done because the first expansion of a polypyrrole is generally much larger than on later cycles. The original thickness of the polypyrrole film in Fig. 2.10 was 6.5 μm just after synthesis, and, as can be seen in the figure, the thickness of the film does not return to this value once it has been subjected to a redox cycle.

An important issue that becomes apparent after polypyrrole test lines have been reduced and oxidized a few times involves adhesion failure between polypyrrole and the gold seed layer. There is no covalent attachment between the gold film and the electropolymerized polypyrrole, and the polymer tends to detach from the gold after a few redox cycles due to its linear expansion of a few percent relative to the supporting electrode. This is the same problem that also plagues the designers of bilayer actuators, and several solutions involving increased roughness of the gold or other electrode materials have been proposed in the literature. In this work, a novel electrode geometry was used to prevent adhesion failure between polypyrrole and gold in the microvalve design, which will be discussed in the following chapter.

2.4 INTEGRATION OF POLYPYRROLE MICROSTRUCTURES WITH SILICON DEVICES

Polypyrrole test lines described above have been fabricated using photolithography on a planar substrate. This fabrication methodology is fully compatible with semiconductor microfabrication, with the implication that polypyrrole microstructures can be potentially integrated on the same substrate with such semiconductor devices transistors and optical diodes. Such integration opens up a realm of interesting possibilities of using polypyrrole actuators as mechanically active elements integrated on a single chip with electronic control circuitry and optical remote communications and power deliver, with potential applications in microrobotics. Below, a proof-of-concept integration of polypyrrole test lines with electrochemically controlled thickness and a silicon pn junction that can function as a photodiode is described. Connection to the pn junction allowed optical control of actuation, potentially enabling microfluidic and lab-on-chip devices which could be remotely controlled by a laser or a photodiode across a layer of biological fluid.

2.4.1 Fabrication of an Optically Controlled Microactuator. An n-type Si wafer with an implanted p-type top layer was used as a substrate. A thin metal film was deposited and patterned on the back and front sides of the substrate. A thin layer of SiO₂ was then sputtered and patterned on the front side of the wafer to protect

exposed Si surface from contact with solution.

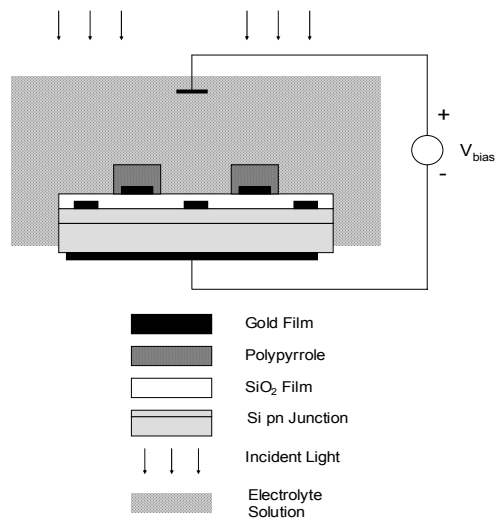


Figure 2.11 Operation of PPy Microactuator Integrated with Si Photodiode

A second layer of metal was deposited and patterned into 50 μm wide strips on top of the oxide layer to provide a seed layer for PPy deposition. The two metal layers and oxide layer were patterned such that both metal films were electrically connected, thus providing PPy with an electrical contact to the p-doped side of the photodiode. PPy was electrochemically deposited on the seed layer from an aqueous solution of pyrrole monomer to a thickness of 4 μm .

2.4.2. Operation of the Microactuator. The finished device was placed in an aqueous solution of NaDBS and biased at $V_{bias} = 2.25\text{V}$ (Figure 1). The displacement of the PPy in the direction normal to substrate surface was then measured by a profilometer as incident light was first switched on and then off.

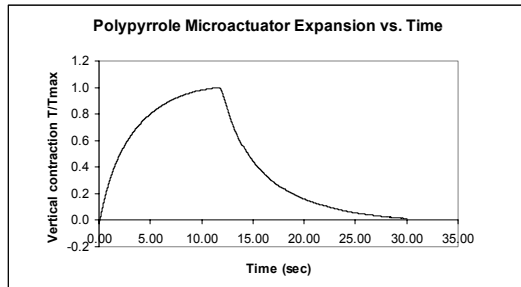


Figure 2.12. Modulation of PPy expansion/contraction with incident light

The maximum contraction/expansion of the actuator due to light modulation (T_{\max}) was measured to be ~ 90 nm, which is $\sim 2\%$ of the PPy thickness as deposited. As can be seen from Figure 2, the time response of the microactuator (τ) is approximately 10 seconds. The time response of the electrochemically actuated polypyrrole depends primarily on mass transport through the polymer matrix, in this case diffusion of Na^+ ions. It follows that if the actuator is scaled down the diffusion time should decrease as well. In the following chapters, a method to fabricate a nanostructure of polypyrrole rods with diameter of 200 nm is shown. This structure would have a time constant at least 2 orders of magnitude smaller than the microactuator, bringing it closer to the time response of biological muscle (10-100 ms).

2.5 ACKNOWLEDGEMENTS

The research described here was supported under funding by AFOSR MURI program. The text of Chapter 2 is, in part, a reprint of the material as it appears in Y. Berdichevsky, Y.-H. Lo, *Lasers and Electro-Optics Society, The 17th Annual Meeting of the IEEE*, Vol. 2, 507-508, 2004. The dissertation author was the primary

researcher and author and the co-author listed in this publication directed and supervised the research which forms the basis of this chapter.

2.6 REFERENCES

1. C. Immerstrand, K. Holmgren-Peterson, et al., "Conjugated-Polymer Micro- and Milliactuators for Biological Applications," *MRS Bulletin*, June 2002, pp. 461-464.
2. E. Smela and N. Gadegaard, *J. Phys. Chem. B*, 105 (39), pp. 9395-9405, 2001.
3. Y. Berdichevsky, Y.-H. Lo, "Polymer Microvalve Based on Anisotropic Expansion of Polypyrrole," *Mat. Res. Soc. Symp. Proc.*, Vol. 782, pp. A4.4.1-A4.4.7, 2004
4. C. R. Martin, "Template Synthesis of Electronically Conductive Polymer Nanostructures," *Acc. Chem. Res.*, 28, pp. 61-68, 1995.
5. E. Smela, *J. Micromech. Microeng.* 9, pp. 1-18, 1999.
6. K. West, L. Bay, M. M. Nielsen, Y. Velmurugu and S. Skaarup, "Electronic Conductivity of Polypyrrole-Dodecyl Benzene Sulfonate Complexes," *J. Phys. Chem. B*, 108, 15001-15008, 2004.
7. L. Bay, T. Jacobsen, S. Skaarup, and K. West, "Mechanism of Actuation in Conducting Polymers: Osmotic Expansion," *J. Phys. Chem. B*, 105, 8492-8497, 2001.
8. T. F. Otero, H.-J. Grande, and J. Rodriguez, "Reinterpretation of Polypyrrole Electrochemistry after Consideration of Conformational Relaxation Processes," *J. Phys. Chem. B*, 101, 3688-3697, 1997.
9. X. Ren and P. G. Pickup, "Ion Transport in Polypyrrole and a Polypyrrole/Polyanion Composite," *J. Phys. Chem.*, 97, 5356-5362.

CHAPTER 3

Polymer Microvalve Based on Anisotropic Expansion of Polypyrrole

3.0 ABSTRACT

An actuator fabricated from the conductive polymer polypyrrole using microfabrication techniques is presented. This actuator utilizes the anisotropic volume change, which occurs under application of an electric field in polypyrrole grown in the presence of NaDBS. This volume change is in direction normal to the substrate, and is several times larger than lateral volume change utilized in polypyrrole microactuators to date. The actuator is applied in a microfluidic valve where membrane and microchannels are fabricated from a transparent elastomer using soft lithography. The use of elastomer enabled a good valve seal and encapsulation of the electrolyte used for polypyrrole actuation.

3.1 INTRODUCTION

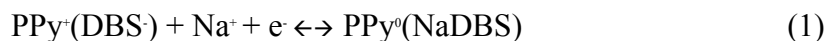
Conducting polymers, distinguished by conjugated polymer backbones, are used for a variety of applications, including fabrication of photonic and electronic devices such as LEDs, transistors, and chemical sensors [1, 2]. Some conducting polymers, such as polypyrrole, have also been used as actuators, or as “artificial muscles” [3].

Under the stimulus of an electric potential, polypyrrole undergoes a reduction-oxidation reaction involving movement of ions in and out of the polymer matrix. This migration of ions leads to volume change. Most commonly, the volume change is converted into mechanical work by employing a bilayer structure, typically a film of

polypyrrole a few tens of micrometers thick on a conducting flexible substrate. When the polymer expands or contracts, the bilayer bends, and electrochemical energy is converted into mechanical energy. These polypyrrole bilayers have been employed at both macro- and micro- dimensions [4], and it has been shown that the volume change in polypyrrole of 2-3% along the surface of the bilayer can produce very large displacement. However, there are a few problems associated with this mode of actuation. The mechanical force that can be applied by the tip of the bilayer, which is the point that undergoes the most physical displacement, is very small – some orders of magnitude smaller than the pressure generated in the polypyrrole film. Also, delamination of the polymer from the substrate is very common, since the bonding between polymer film and electrode is mostly due to noncovalent interactions [5]. It has been reported in the literature that polypyrrole electropolymerized in the presence of sodium dodecylbenzenesulfonate (NaDBS), can undergo reversible volume change of 30% or more in the direction normal to the substrate [6]. The authors hypothesized that this is due to anisotropic morphology of polypyrrole (PPy) film with incorporated DBS ions. This volume change, if realized in a thick micropatterned PPy film, can be directly applied in a variety of micromechanical systems. In this work, a microvalve utilizing anisotropic volume change of PPy(DBS) is fabricated.

3.2 CONCEPT

A typical microfluidic system for such applications as a lab-on-a-chip or remote sensing will utilize relatively long microchannels with width and depth of only a few tens of micrometers or less. Typical fabrication materials include glass, quartz, silicon as well as polymer materials such as polycarbonate and polymethylmethacrylate (PMMA) [7]. Also, a high number of microfluidic devices are fabricated using polydimethylsiloxane (PDMS), which is a transparent elastomer [8]. This material has many attractive optical and mechanical properties, and can be easily molded and bonded at temperatures less than 100° C. One property that is particularly useful in the design of a microvalve is that it is possible to fabricate thin PDMS membranes by spin-coating technique. These membranes are very flexible and form a non-permanent watertight seal when pressed against another smooth surface. Therefore, the valve design reported here is implemented with a PDMS microfluidic system consisting of two chambers: working channel for biological or chemical analyte separated by a thin PDMS membrane from the electrolyte bath containing the polypyrrole microactuator and a gold counter electrode. (See Figure 1). This valve operates as follows: an application of voltage between working electrode (WE), consisting of PPy(DBS) deposited on a gold conductor, and counter electrode (CE), which is a patterned gold film, produces a red-ox reaction involving Na⁺ ions in the electrolyte. This reaction can be represented by the following equation:



As ions move into the polymer, it swells and pushes the membrane separating two chambers into the working channel. This seals the working channel completely, resulting in a closed state for the valve. Under application of reverse voltage, polymer shrinks, allowing the PDMS to come back into original position, thus opening the working channel.

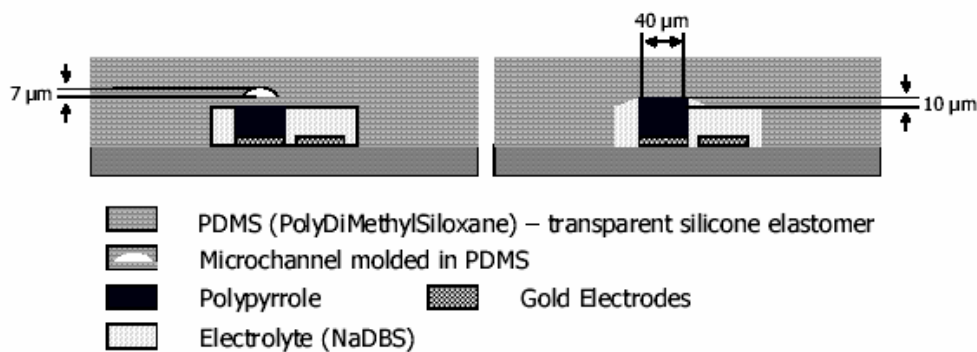


Figure 3.1 Proposed Microvalve. Working channel is open on the left, and is closed by the expanding polypyrrole on the right.

It should be noted that depositing PPy(DBS) on a flat gold electrode results in a very significant problem. After 2 or 3 cycles, the polymer completely delaminates from the electrode due to swelling parallel to the substrate, which happens simultaneously with volume change normal to the substrate. As discussed earlier, this lateral volume change is far smaller than the one in the vertical direction, but it is enough to detach the polymer from the substrate. For this reason, polypyrrole was deposited on electroplated gold posts of 8-9 μm height. (See Figure 2) These posts were electroplated through photoresist wells, resulting in a T-shaped cross-section. Polypyrrole was then electropolymerized on these posts, completely surrounding them, which reduced the possibility of delamination during operation. In addition, the

gold posts were left with a rough top surface, which further improved adhesion between gold and polypyrrole.

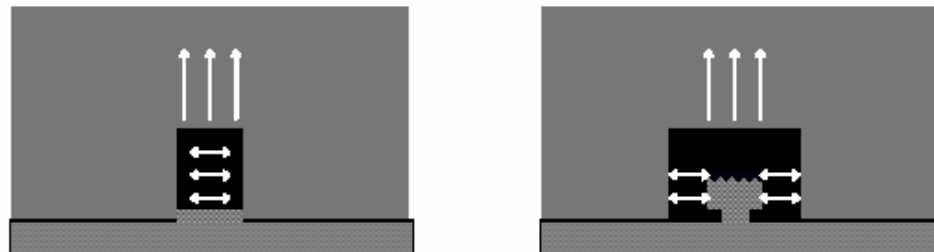


Figure 3.2 Forces exerted by expanding polypyrrole are represented as arrows. In schematic on the left, the lateral forces aren't countered, and will result in delamination after few cycles. In schematic on the right, the lateral forces are countered by Au post.

3.3 EXPERIMENT

3.3.1 Microfabrication of the Active Part of the Microvalve. The active component in this microvalve is the polypyrrole microactuator. The microfabrication process sequence on a glass substrate is as follows. (See Figure 3)

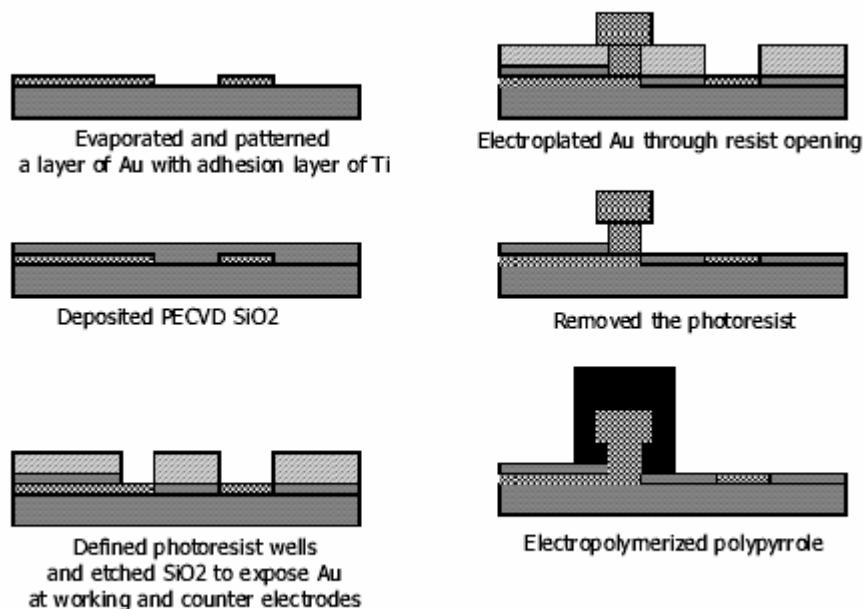


Figure 3.3 Microfabrication process for polypyrrole actuator.

First, an adhesion layer of Ti (10 nm) is thermally evaporated onto a glass substrate. Then, a conducting film of gold of 400 nm thickness is thermally evaporated on top of Ti, and both metals are photolithographically patterned to form working and counter electrodes as well as metal traces to contact pads. An insulating silicon dioxide film 500 nm thick is deposited via PECVD. SU-8(5) photoresist is then spin-coated onto the oxide to a thickness of 2 μm , exposed and developed to open up resist wells over the electrodes. The exposed area of the working electrode is a 40 μm square, while the exposed area of the counter electrode is a 40 μm wide semi-circular strip surrounding the working electrode. Oxide in these wells is etched away, and more gold is electroplated in the working electrode well to produce the round T-shape with

rough surface discussed above. It was experimentally determined that electroplated Au posts need to be at least 8-9 μm high to provide good mechanical support for the polypyrrole. The photoresist is then stripped away using oxygen plasma etching, and the chip is ready for electropolymerization of polypyrrole. An aqueous solution of 0.04M pyrrole and 0.04 NaDBS is prepared, and the polypyrrole is deposited onto the working electrode at 0.62 V (vs. Ag/AgCl counter electrode) using a potentiostat (Gamry PCI-300). Polymerization time is 4.3 hours, resulting in a PPy(DBS) thickness of 34 μm on top of the gold post. Polypyrrole grows laterally as well, at roughly the same rate, producing a pattern width of around 110 μm (gold post width is 40 μm , and has ~ 35 μm of polypyrrole surrounding it). This growth is not uniform, and the resulting pattern isn't symmetrical. Rather, it appears that polypyrrole growth follows slight imperfections in the substrate surface.

3.3.2 Microfabrication of the passive microfluidic component. A technique known as soft lithography was utilized in the fabrication of PDMS microchannels. Briefly, the working channel was made by photolithographically defining AZ P4620 resist (Clariant) of 6.2 μm thickness into 50 μm -wide and 20 mm-long strips making a Y-shape on silicon substrate. The photoresist was then re-flowed at 150° C for 20 minutes, producing a spherical cross-section (the resist cross section was originally rectangular). (See Figure 4) A pre-polymer of PDMS (Dow Corning, Sylgard 184) was then mixed at 10:1 ratio with a cross-linking agent (Dow Corning), degassed in vacuum, and poured onto the silicon wafer with photoresist pattern. After

curing PDMS at 65° C for 4 hours, the fully cross-linked PDMS was peeled off the silicon mold master by hand, and cut into chip-sized pieces.

An analogous method was used to make the microchannel that would act as an electrolyte bath. SU-8(50) photoresist (Microchem) was spin-coated onto a silicon wafer at 2500 rpm, resulting in a 41 μm thickness. The photoresist was then patterned according to manufacturer supplied parameters, making 100 μm -wide and 20 mm-long strips with a wider area (0.5 mm at the widest point) in the middle to accommodate the actuator with counter electrode and electrolyte bath.

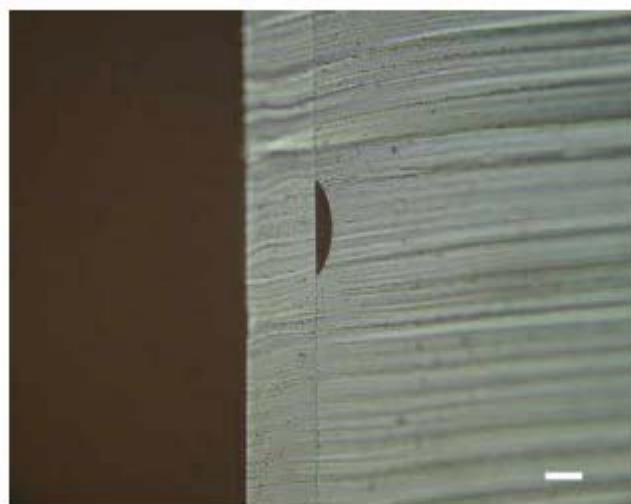


Figure 3.4 Micrograph of the cross-section of the working microfluidic channel molded against reflowed photoresist and sealed with PDMS membrane. Bar represents a distance of 20 μm .

PDMS was then mixed as described above, spin-coated onto this mold master at 1000 rpm, and then heat cured as above. This produces a PDMS membrane about 85 μm thick in the areas free of resist, and 44 μm thick on top of the SU-8(50) pattern. A piece of PDMS containing the Y-shaped working channel was then bonded to the

PDMS membrane still on the silicon wafer by exposing both to oxygen plasma at 75W and 200mT flow-rate for 10 seconds (Technics PEIIB Plasma Etcher) and pressing them together after visual alignment on a mechanical stage. The PDMS assembly was then demolded from the second silicon master.

The final step of the process was to drill fluid access holes in the PDMS assembly, and align it with the active PPy actuator on the glass substrate. (See Figure 5).

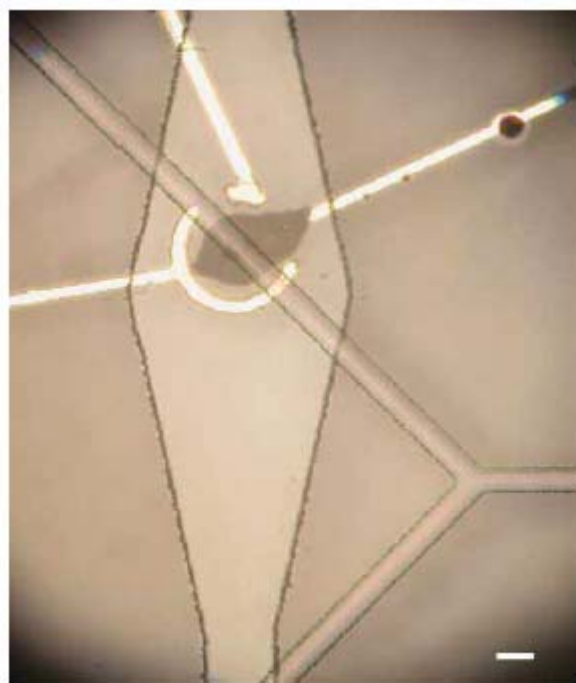


Figure 3.5 Micrograph of the top view of fully assembled microvalve including the active component with electrodes and metal traces (bright lines), rhombus-shaped electrolyte bath, and Y-shaped working channel. The valve is placed under one of the arms of the Y, preventing the analytes flowing in that channel from merging with contents of the other arm of the Y. The bar represents a distance of 50 μm .

Plasma bonding wasn't used in this step, since pressing PDMS against a glass surface produces a reversible water-tight seal and enables reuse of either passive or active part of the device. The electrolyte channel was then filled with 0.1 M aqueous solution of

NaDBS, and voltage was applied between working and counter electrodes to produce a change in volume of the PPy(DBS) actuator.

3.4 RESULTS

Actuation was carried between $V_{we} - V_{ce} = -2.6$ V and $V_{we} - V_{ce} = 0.0$ V, which roughly correspond to -1 V and 0 V vs. an Ag/AgCl reference. Voltage was limited to these values because hydrogen bubbles start to form below -2.6 V and it is possible to permanently damage the polymer above 0 V. It became apparent that it would be highly desirable to have a reference electrode integrated on-chip next to the micro-actuator to enable application of accurate voltages, as the voltage between working and counter electrodes drifted occasionally. Nevertheless, despite the lack of integrated reference electrode, it was possible to close and open the working channel. (See Figure 6) As can be seen from the picture, the hemispherical crosssection of the channel enabled a complete seal at the maximum volume increase in the PPy(DBS) actuator. The operation was then quantitatively verified under a profilometer (Dektak 3030) using an open PDMS electrolyte bath with no microchannel, allowing access for the profiling stylus. The actuation proceeded as follows: first, the polymer expanded to the thickness of 45 μ m from the original thickness of 34 μ m, with 32% vertical volume change, after application of $V_{we-ce} = -2.6$ V. Under subsequent application of $V_{we-ce} = 0.0$ V, the polypyrrole

shrank back to 41 μm . It was then possible to reversibly change the height of the actuator

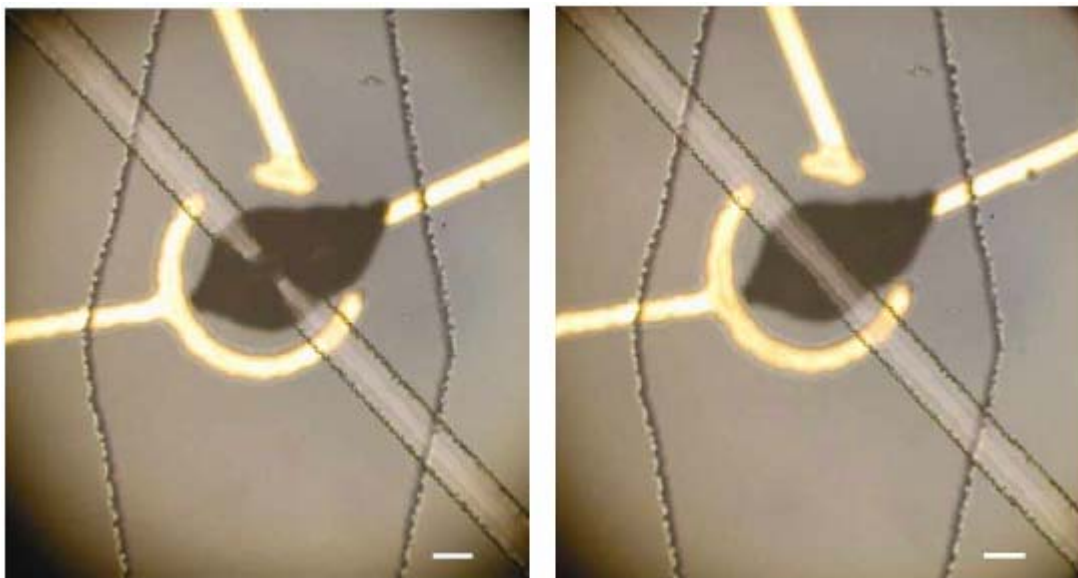


Figure 3.6 Closed valves on the left, and open valve on the right. Expanding polypyrrole (dark material between Au traces) can be seen to pinch off the working channel in left micrograph. The bar represents a distance of 50 μm .

between 41 μm and 45 μm by alternating the voltage between -2.6 and 0 V (although not always returning to the same height due to voltage drifts in the absence of reference electrode). Thus, the reversible volume change in direction normal to the substrate is 12% of the original volume. This volume change took 10-15 seconds. This volume change is significantly lower than that reported for a continuous thick PPy film or a micropatterned thinner film (1-1.5 μm) – 80% non-reversible original volume change, and 30% subsequent reversible volume change. This is likely due to fabrication method used –instead of growing the polypyrrole on a flat substrate, it was grown on a protruding gold post to prevent delamination. It is possible to hypothesize that anisotropic morphology of PPy is oriented normal to the substrate, and is thus

actually oriented parallel to wafer surface in PPy surrounding the post, while oriented normal to the wafer surface in PPy on top of the post. Thus, the large volume change occurs not only in the normal direction, but also in the lateral direction in the Au post design. This was confirmed by video microscopy, which showed reversible lateral volume expansion increasing the diameter of PPy actuator by 4 μm , or 6% - about half of the volume expansion in the normal direction, but still much larger than lateral expansion in PPy films grown conventionally on a flat substrate.

3.5 CONCLUSION

A microvalve utilizing a previously little-explored mode of actuation of polypyrrole was microfabricated and successfully operated. Feasibility of fabricating small area active polymer devices that are capable of producing large mechanical displacements while utilizing very few moving parts was demonstrated.

3.6 ACKNOWLEDGEMENTS

The research described here was supported by funding for AFOSR MURI program. The text of Chapter 3 is, in part, a reprint of the material as it appears in Y. Berdichevsky, and Y.-H. Lo, *Mat. Res. Soc. Symp. Proc.* Vol. 782, A4.4.1-A4.4.7, 2004. The dissertation author was the primary researcher and author and the co-author

listed in this publication directed and supervised the research which forms the basis of this chapter.

3.7 REFERENCES

1. J. W. Gardner, P. N. Bartlett, *Sensors and Actuators A* **51**, 57-66 (1995).
2. Q. Pei, G. Yu, C. Zhang, Y. Yang, A. J. Heeger, *Science* **269**, 1086 (1995).
3. R. H. Baughman, *Synthetic Metals* **78**, 339-353 (1996).
4. E. Smela, *J. Micromech. Microeng.* **9**, 1-18 (1999).
5. X. Cui, D. C. Martin, *Sensors and Actuators A* **103**, 384-394 (2003).
6. E. Smela and N. Gadegaard, *J. Phys. Chem. B*, **105** (39) 9395-9405, 2001; *Advanced Materials*, **11** (11) 953-7, 1999.
7. M.J. Madou, *Fundamentals in Microfabrication*, (CRC press, 1997).
8. D. Duffy, J.C. McDonald, J.A. Schueller, G.M. Whitesides, *Anal. Chem.* **70**, 4974-4984, 1998.

CHAPTER 4

Fabrication of Polypyrrole Nanowires

4.1 ABSTRACT

An artificial muscle composed of electroactive nanowires or nanofibers would compare favorably to its biological counterpart in terms of generated force and speed, while devices based on discrete nanoactuators could perform functions similar to those of motor proteins in biological cells. A template synthesis method for producing polypyrrole nanowires is examined. Conductivity and electrochemical properties of resulting nanowires are evaluated, showing promise for future use as nanoactuators. Template synthesis is then extended to allow fabrication of polypyrrole nanowires directly on a planar substrate such as semiconductor wafer, enabling potential integration with semiconductor or microfluidic devices.

4.2 INTRODUCTION

Conducting polymers such as polypyrrole have been studied for applications as actuators and artificial muscles for a number of years [1-5]. One useful metric for evaluating such devices is to compare them with biological muscle. Biological muscle can undergo contractions of more than 20% of its length with a time response measured in tens of milliseconds. Biological muscle is a rather complicated hierarchical machine with mechanically active nano components in the form of proteins. Hierarchical organization allows muscle to avoid diffusion limitations for

providing both fuel (oxygen and ATP) and signaling (small ions) to its proteins.

Parallel operation of bundles of proteins nanofibers allows muscle to achieve its strong contraction. This complex structure stands in contrast to design of artificial muscle actuators, which are typically composed of a homogeneous material. If an artificial muscle material such as polypyrrole could be fabricated at the nanoscale and operated as a nanoactuator, we could imagine mimicking the hierarchical structure of biological muscle using polypyrrole nanowires as building blocks. Furthermore, such nanoactuators could find applications when used as stand-alone devices, again mimicking the performance of biological nano and microactuators such as motor proteins, cell cilia, or flagella.

In this chapter, a template synthesis methodology for fabrication of polypyrrole nanowires is demonstrated. Template synthesis has been used to synthesize polypyrrole in nano-sized pores of a variety of commercially available and custom-made membranes [6-11]. This technique is extended to fabricate polypyrrole nanofibers doped with dodecylbenzenesulfonate (DBS). First, nanowires were fabricated using a commercially available alumina membrane to test their electrical and electrochemical properties. Then, nanowires were synthesized directly on a semiconductor substrate using an anodized alumina film as a template.

4.3 EXPERIMENT AND DISCUSSION

4.3.1 Template synthesis in stand-alone membranes Template synthesis methodology for synthesis of polypyrrole (PPy) nanowires described previously in the

literature [12] was used in this work with minor modifications. A 300 nm gold film was sputtered onto a 0.2 μm porous alumina membrane (Whatman) to provide the seed layer for electropolymerization of polypyrrole. The membrane was then mounted on a glass cover slip, and its edges sealed with thermal wax to prevent backside polymerization (Figure 4.1).

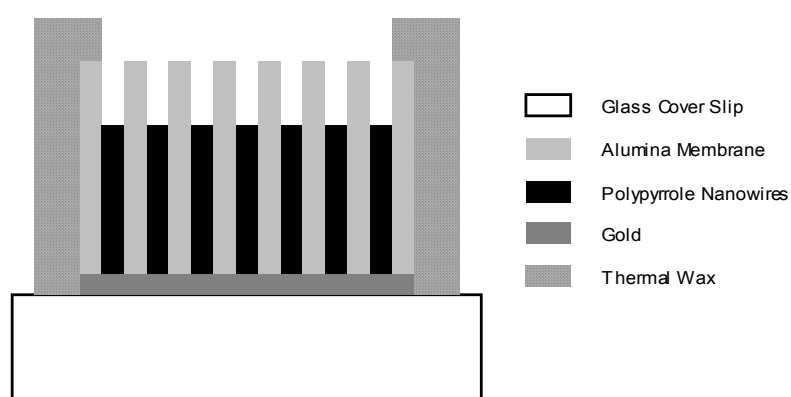


Figure 4.1. Polypyrrole nanowire template synthesis

Polypyrrole was electropolymerized from a solution of 0.1 M pyrrole (Sigma-Aldrich) and 0.1 M sodium dodecylbenzenesulfonate (NaDBS, Aldrich) at 0.55 V versus an Ag/AgCl reference electrode for 2 hours using the Gamry PCI4-300 potentiostat. The sample was then removed from the solution, washed with deionized water, and placed for 40 minutes in a 0.2 M sodium hydroxide (NaOH) solution to dissolve the alumina. The sample was then cut and observed with FEI Company Quanta 600 scanning electron microscope (SEM) to provide top (Figure 2a) and side

views (Figure 2b). From the SEM micrographs it can be seen that the nanowires are approximately 20 micrometers in length and 220 nm in diameter on average. The top of the nanowires is in fact a hollow tube; however, it is unclear if the nanowire is hollow along its entire length.

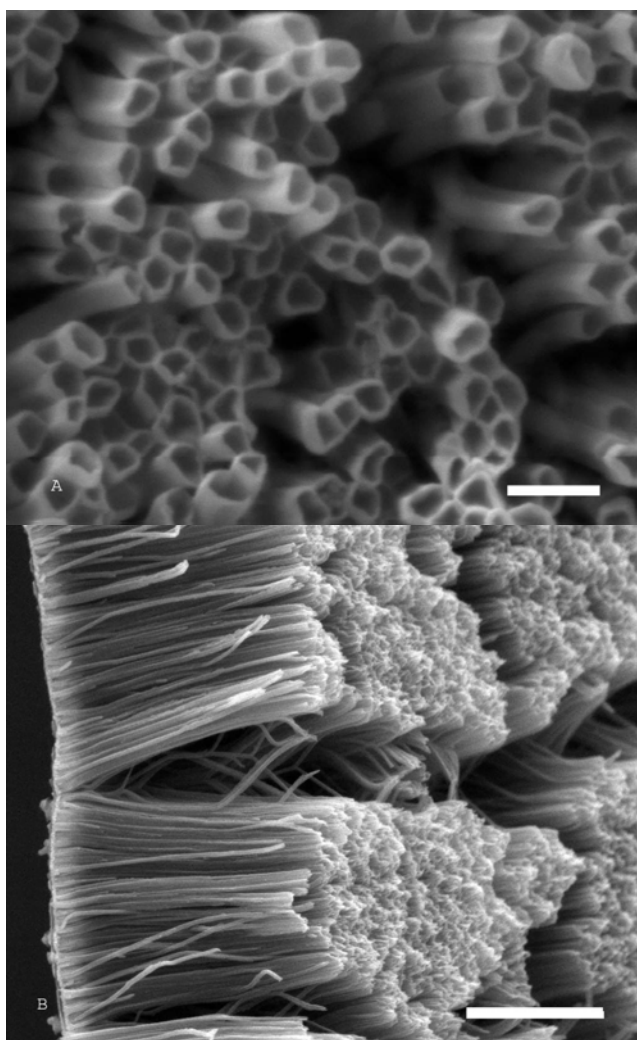


Figure 4.2. Figure 4.2a is the top view and Figure 4.2b is the side view of 20 μm long 220 nm nanowires. Scale bar in Figure 4.2a is 500 nm, and 10 μm in Figure 4.2b.

Exposure of polypyrrole to a strong alkaline solution during dissolution of alumina membrane can affect polypyrrole's electrochemical properties. It has been

proposed in the literature that the mechanism for this change could involve displacement of the dopant ions in the polymer matrix by hydroxide. Since DBS is a bulky ion that is immobile in the polypyrrole matrix, this effect should be minimized in PPy(DBS). To test this hypothesis, a cyclic voltammogram of the sample was taken in a 0.1 M NaDBS solution at 2 mV/sec scan rate (Figure 4.3). In a polypyrrole doped with DBS anions, a reduction and an oxidation peak should be prominent. In Figure 4.3, we can see that this is indeed the case; the flattening of the curve observed when polypyrrole films doped with ions such as BF_4^- were exposed to NaOH solution [12] didn't occur. This is a promising sign for suitability of PPy(DBS) nanowires synthesized in this manner for use as nanoactuators: the redox peaks correspond to movement of sodium ion in and out of the polymer matrix, leading to volume change that can be harnessed for actuation.

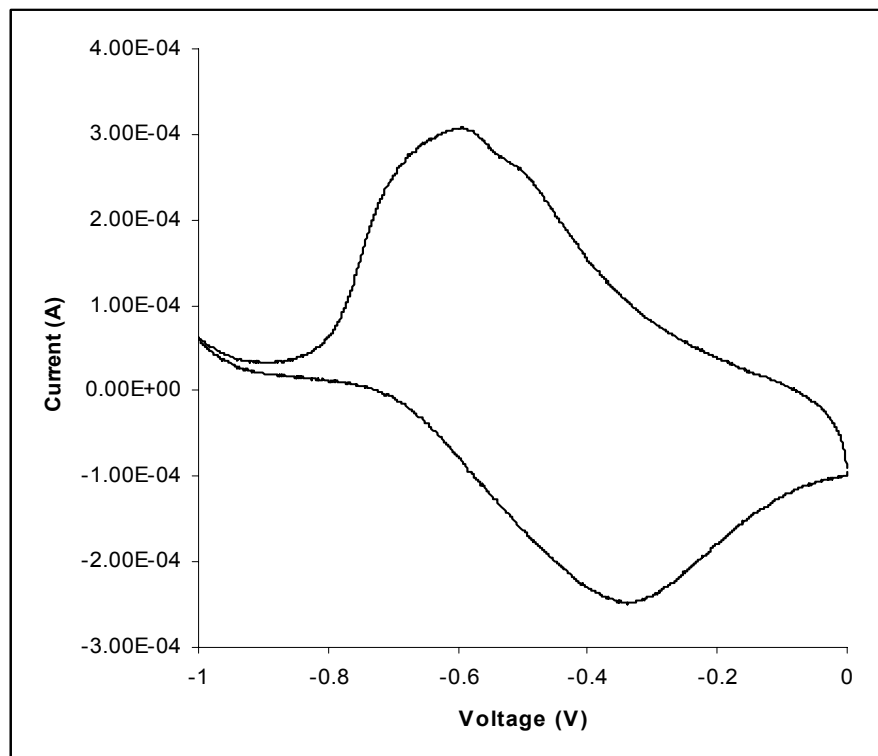


Figure 4.3. Cyclic voltammogram of PPy(DBS) nanowires showing redox peaks

4.3.2 Fabrication of discrete nanowires. Next, we developed a procedure for making discrete nanowires that could be used for individual electrical or mechanical testing. Polypyrrole was polymerized as described above, and the alumina membrane containing the nanowires was removed from the glass slide by dissolving thermal wax in acetone. The membrane was then mounted on a steel chuck with gold side facing up, and the gold film was removed by brief mechanical lapping of the membrane with abrasive 9 μm alumina powder. The lapping was stopped once all gold was removed, as determined by visual inspection. The membrane was then dismounted from the chuck, washed with deionized water, and placed in a small volume (1.5 mL) test tube

filled with 0.2 M NaOH solution for 40 minutes to dissolve the alumina. Next, the test tube was centrifuged at 10,000 rpm for 30 seconds to collect all the nanowires at the bottom, and refilled with deionized water. This step was repeated three times to make sure all of the NaOH was gone and the solution was at neutral pH.

We tested the nanowires' electrical conductivity by depositing a droplet (20 μL) of solution containing the nanowires onto a glass substrate photolithographically patterned with gold lines 50 μm wide spaced at various intervals between 5 and 25 μm . Upon drying, some of the nanowires would end up immobilized across the gap between two adjacent gold lines with an overlap on either side (see Figure 4).

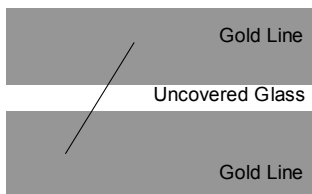


Figure 4.4. A schematic showing a PPy(DBS) nanowire (black line) spanning the gap between two micropatterned gold lines.

By measuring the resistance between the gold lines and the nanowire length over insulating glass region, it was possible to obtain the individual nanowire conductivity. This measurement was performed a number of times on a few different nanowires to determine average conductivity (Table 1). Conductivity was calculated assuming a circular and solid nanowire cross-section with a diameter of 225 nm.

Table 4.1. Average Conductivity = $0.33 \text{ S} \cdot \text{cm}^{-1}$

Length of Nanowire Over Glass (μm)	Measured Resistance (Ω)	Calculated Conductivity ($\text{S} \cdot \text{cm}^{-1}$)
13	8.8 M	0.37
11	10.2 M	0.27
14	10 M	0.35
15	11 M	0.34

This conductivity ($0.33 \text{ S} \cdot \text{cm}^{-1}$) is one to two orders of magnitude lower than values reported for polypyrrole films in the literature and values measured in our lab, raising two possibilities. One is that contact resistance dominates measured resistance; however, it would seem likely that conductivity values would vary widely if that were the case. In the data reported, while some variation is observed even after taking lengths of the nanowires into account, it doesn't seem to explain the large difference between nanowire and film conductivities. The other possibility is that a significant portion of the nanowire is hollow, as described above, which would imply that the actual cross-section of the nanowire is much smaller than one assumed in the calculation above.

4.3.3 Alumina anodization and nanowire electropolymerization on a semiconductor substrate. In order to make integration of polypyrrole nanostructure with semiconductor devices straightforward, a method is needed to synthesize

nanowires directly on a planar substrate. This would enable photolithographic patterning of regions where nanowires are polymerized and would thus allow integration with any electronic, photonic, or microfluidic devices on the same substrate. To make this possible, the template used for producing nanowires needs to be fabricated in-situ on insulator or semiconductor substrates used in microlithography.

Alumina (Al_2O_3) anodization on an insulating substrate was reported previously for pattern transfer to silicon [13] and for template synthesis on silicon wafers and glass [14]. This procedure was adopted for our work with some modifications. Briefly, a silicon wafer with a 10,000 Å layer of thermal oxide was used as a substrate. A 400 nm titanium film was sputtered onto the substrate, followed by thermal evaporation of aluminum films of various thicknesses (500 nm – 1500 nm). The wafer was cut into chips, which were then placed in a custom made chuck which protected the chip's backside while providing an electrical connection to the aluminum front-side. Aluminum was then anodized under three different conditions: at 50 V in a 15°C 0.3 M oxalic acid, at 170 V in 4°C in 0.5 M phosphoric acid, and at 280 V in 4°C 0.5 M tartaric acid versus a stainless steel counter-electrode. The cross-sections of these three samples were examined under SEM and are shown in Figures 5 a-c, respectively. As can be seen in the figures, these three different anodization conditions give widely ranging pore sizes and spacing, from 85 nm pore spacing in Figure 4.5a to 220 nm pore spacing in Figure 4.5b and finally 450 nm pore spacing in Figure 4.5c. A significant problem in utilizing these porous alumina layers for

template synthesis becomes apparent upon examination of the micrographs – the pores don't extend all the way to the conducting titanium layer, but rather terminate in an insulating barrier layer of alumina when anodization is finished. This barrier layer can be removed by immersing the sample in a solution of phosphoric acid; however, phosphoric acid etches alumina isotropically and will significantly widen the pores depending on the etch time. Therefore, if small pore size is to be preserved, an anisotropic etching method has to be used. In this work, we dry etched the barrier layer using a boron trichloride (BCl_3) and argon (Ar) gas mixture in a Trion RIE/ICP reactor. The sample was etched for 300 seconds at 550 Watts with 4 sccm Ar flow and 10 sccm BCL_3 flow, anisotropically removing 520 nm of Al_2O_3 from both the top of the porous layer and from the bottom of the pores. Since the barrier layer was approximately 300 nm thick, it was removed completely. The etch stopped once the underlying titanium was exposed. After the dry etch, polypyrrole was electropolymerized in the alumina pores and alumina was dissolved as described

above. The resulting polypyrrole nanowires are shown in Figure 4.5d.

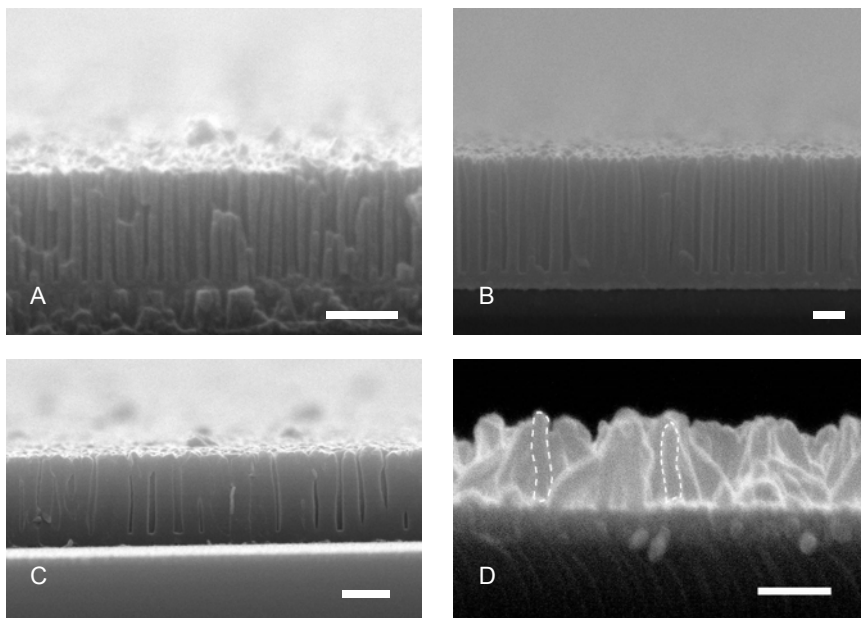


Figure 4.5 Cross sections of alumina anodized on planar substrates under different conditions, A-C, and a side view of polypyrrole nanowires electropolymerized using template synthesis, D. Scale bars are 500 nm in A, B, and D, and 1 μ m in C.

In this work, we anodized the porous alumina film over the entire wafer surface; however, this technique can be extended to anodizing microlithographically defined aluminum islands or arrays, in which polypyrrole nanowires can be polymerized. This would free large areas of the substrate for fabrication of a wide variety of available semiconductor devices that could be electrically connected to nanowires, thus enabling close integration of these two very different technologies.

4.3.4 Heterostructure nanowires We have also extended the template synthesis technique to fabricate polypyrrole-gold heterostructure nanowires. The ability to make heterostructure actuators can potentially be very useful, both for providing good electrical contacts to nanoactuators, and for allowing more complex

mechanical motion. Heterostructures can be easily synthesized by alternating electroplating and electropolymerization solutions as many times as

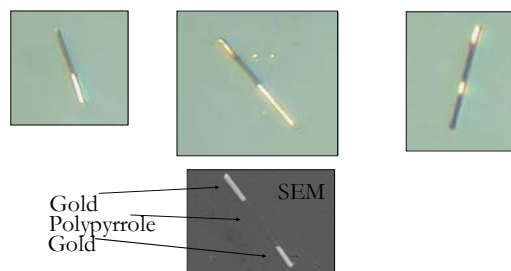


Figure 4.6. Gold – polypyrrole heterostructure nanowires. Top three images are optical micrographs of nanowires with different layer structure, the bottom image was taken with SEM.

necessary to deposit layers of different materials in the nanopores of the template.

Here, we alternated a gold plating solution and a pyrrole-NaDBS

electropolymerization solution to produce nanowires shown in Figure 6.

4.4 CONCLUSION

Above, a fabrication methodology for producing alumina nanowires in the discrete form and integrated on a planar substrate was presented. It was found that template synthesis of a PPy(DBS) results in nanowires which preserve conductivity and electrochemical properties of PPy(DBS) films which function as artificial muscles. Thus, such nanowires show potential to be used as either nano building blocks of larger actuation systems, or as discrete nano-actuators to be used individually and perhaps together with integrated microfluidic and/or semiconductor devices. To enable such integration, we developed a technique which allows

electropolymerization of polypyrrole nanowires directly on a planar substrate such as a semiconductor wafer. It is thus possible to envision nanoactuators being synthesized directly on wafers or chips holding electronic devices such as amplifier and/or logic components, photoelectronic devices like light-emitting diodes (LEDs) and photodetectors, and microfluidic or MEMS components. To realize this promise, we are working on examining the structure and the mechanical properties of polypyrrole nanowires and on improving the fabrication techniques.

4.5 ACKNOWLEDGEMENTS

This research was supported by funding under AFOSR MURI program. The text of Chapter 4 is, in part, a reprint of the material as it appears in Y. Berdichevsky, and Y.-H Lo, *Smart Structures and Materials 2005: Electroactive Polymer Actuators and Devices, Proc. SPIE* Vol. 5759, 268-273, 2005. The dissertation author was the primary researcher and author and the co-author listed in this publication directed and supervised the research which forms the basis of this chapter.

4.6 REFERENCES

1. Q. Pei and O. Inganäs, "Electrochemical Applications of the Bending Beam Method. 2. Electroshrinking and Slow Relaxation in Polypyrrole," *J. Phys. Chem.*, 97, 6034-6041, 1193.
2. T. F. Otero and J. M. Sansiñena, "Artificial muscles based on conducting polymers," *Bioelectrochem. Bioen.*, 38, 411, 1995.
3. R. H. Baughman, "Conducting polymer artificial muscles," *Synthetic Metals*, 78, 339-353, 1996.

4. E. Smela, "Microfabrication of PPy microactuators and other conjugated polymer devices," *J. Micromech. Microeng.*, 9, 1-18, 1999.
5. C. Immerstrand, K. Holmgren-Peterson, K.-E. Magnusson, E. Jager, M. Krogh, M. Skoglund, A. Selbing, and O. Inganäs, "Conjugated-Polymer Micro- and Milliactuators for Biological Applications," *MRS Bulletin*, June, 461-464, 2002.
6. C. R. Martin, R. Parthasarathy, and V. Menon, "Template Synthesis of Electronically Conductive Polymers – a New Route for Achieving Higher Electronic Conductivities," *Synthetic Metals*, 55-57, 1165-1170, 1993.
7. C. R. Martin, "Template Synthesis of Electronically Conductive Polymer Nanostructures," *Acc. Chem. Res.*, 28, 61-68, 1995.
8. C. Schönenberger, B. M. I. van der Zande, L. G. J. Fokkink, M. Henny, C. Schmid, M. Krüger, A. Bachtold, R. Huber, H. Birk, and U. Staufer, "Template Synthesis of Nanowires in Porous Polycarbonate Membranes: Electrochemistry and Morphology," *J. Phys. Chem. B*, 101, 5497-5505, 1997.
9. S. Demoustier-Champagne and P. Stavaux, "Effect of Electrolyte Concentration and Nature on the Morphology and the Electrical Properties of Electropolymerized Polypyrrole Nanotubules," *Chem. Mater.*, 11, 829-834, 1999.
10. M. Lu, X. Li, H. Li, "Synthesis and characterization of conducting copolymer nanofibrils of pyrrole and 3-methylthiophene using the template-synthesis method," *Materials Science and Engineering*, A334, 291-297, 2002.
11. J. Joo et al., "Conducting Polymer Nanotube and Nanowire Synthesized by Using Nanoporous Template: Synthesis, Characteristics, and Applications," *Synthetic Metals*, 135-136, 7-9, 2003.
12. L. S. Van Dyke and C. R. Martin, "Electrochemical Investigations of Electronically Conductive Polymers. 4. Controlling the Supramolecular Structure Allows Charge Transport Rates To Be Enhanced," *Langmuir*, 6, 1118-1123, 1990.
13. D. Crouse, Y.-H. Lo, A. E. Miller and M. Crouse, "Self-ordered pore structure of anodized aluminum on silicon and pattern transfer," *Applied Physics Letters*, 76, 49-51, 2000.
14. O. Rabin, P. R. Herz, Y. Lin, A. I. Akinwande, S. B. Cronin, and M. S. Dresselhaus, "Formation of Thick Porous Anodic Alumina Films and Nanowire Arrays on Silicon Wafers and Glass," *Advanced Functional Materials*, 13(8), 631-638, 2003.

CHAPTER 5

Polypyrrole Nanowire Actuators

5.1 INTRODUCTION

In recent years, there has been an intensified effort to create nano-sized devices capable of carrying out mechanical work. The work reported in the literature has ranged from top-down fabrication of nano electromechanical actuators with ultraviolet or electron-beam lithography and scanning-probe microscopy manipulation to bottom-up chemical synthesis of molecular machines and DNA motors and harvesting natural biomotors. [1-3] Conducting polymer actuators, such as polypyrrole actuators, are based on expansion and contraction of the polymer matrix with the movement of ions during electrically controlled reversible oxidation and reduction.[4, 5] Polypyrrole can be synthesized in a variety of geometries at macro and micro scales, as well as in the shape of nanowires by utilizing template synthesis in nanopore membranes.[6] In this work, template synthesis was used to fabricate polypyrrole nanowires, and characterized their ability to function as nanoactuators in an aqueous fluid environment. It was demonstrated that conducting polymer nanowires can function as electrically controlled nanoactuators. Bundles consisting of parallel nanowires were employed, which displayed a reversible increase in length of up to 3% that can potentially be converted to a large scale angular movement by employing a bimorph-like structure. Nanowires were further characterized by x-ray scattering and chronoamperometry to elucidate their structure and time response.

Applications of successful nano-machines are potentially numerous and far-reaching, including advances in computation and communications through use of rapidly-switching nanoactuators coupled to mirrors or magnetic storage elements. Nanorobotic devices capable of operating in a fluid environment could be used in biomedical sciences and in health care, allowing small-scale manipulation of flows and particles. Some of the problems encountered in fabrication and operation of nanomechanical devices include potential for mass production, ease of control, and restrictions on operating environment. For example, the use of electron-beam lithography is suitable for fabricating components one at a time, in a serial fashion, and so creating of large numbers of nanoactuators with this method could be prohibitively expensive. On the other hand, chemical synthesis or utilization of naturally occurring nanomotors could allow simultaneous fabrication of large numbers of these devices; however, these motors can be difficult to control and require very restricted operating environments.

In this work, a different approach was undertaken to fabricate nanoactuators. “Artificial muscle” materials, including some conducting and ionic polymers, dielectric elastomers, and other materials, can expand or contract upon application of an electric field or a pH change, and have already been used to create both macro- and micro- actuators. We used a template-synthesis method to shrink the dimensions of a conducting polymer (polypyrrole) actuator to nanoscale to simultaneously synthesize $> 10^8$ (pore density of an anodized alumina template can range from 10^8 to 10^{12} cm^{-2})

artificial muscle nanowires capable of electrically-controlled reversible expansion and contraction.

5.2 POLYPYRROLE NANOWIRE ELECTROPOLYMERIZATION AND EVALUATION OF THE ELECTROCHEMICALLY CONTROLLED VOLUME CHANGE

5.2.1 Removal of Hollow Region of Synthesized PPy Nanowires by Mechanical Lapping. (PPy) films can be synthesized on a conducting surface by electropolymerization, and various dopant ions can be incorporated into the polymer altering many of its properties. In this work, we use polypyrrole doped with dodecylbenzenesulfonate anions (DBS⁻). Oxidation and reduction of PPy(DBS) films can be controlled by applying voltage in aqueous electrolyte solutions, such as a solution of sodium dodecylbenzenesulfonate (NaDBS) salt, and are accompanied by the movement of ions and their hydration shells into the polymer matrix (reduction) or out (oxidation). The movement of ions results in contraction or expansion of the polymer, or actuation, which in turn can be harnessed to perform a useful mechanical function.[7, 8] The PPy(DBS) film expands anisotropically, with 2-3% expansion along the electrode surface, and up to 30% expansion in the direction normal to the surface.[9] Both lateral and normal modes of expansion have been harnessed to make devices by various laboratories, including ours.[10] In template synthesis of PPy(DBS) nanowires, one side of a nanoporous membrane is coated with conducting

material, and then the PPy is electropolymerized through the pores. We used a 60 μm thick alumina membrane with 200 nm diameter pores, resulting in nanowires of the same diameter with a length controlled by polymerization time.[11] As can be seen in Figure 5.1(a), the top portion of the nanofibers is hollow with very

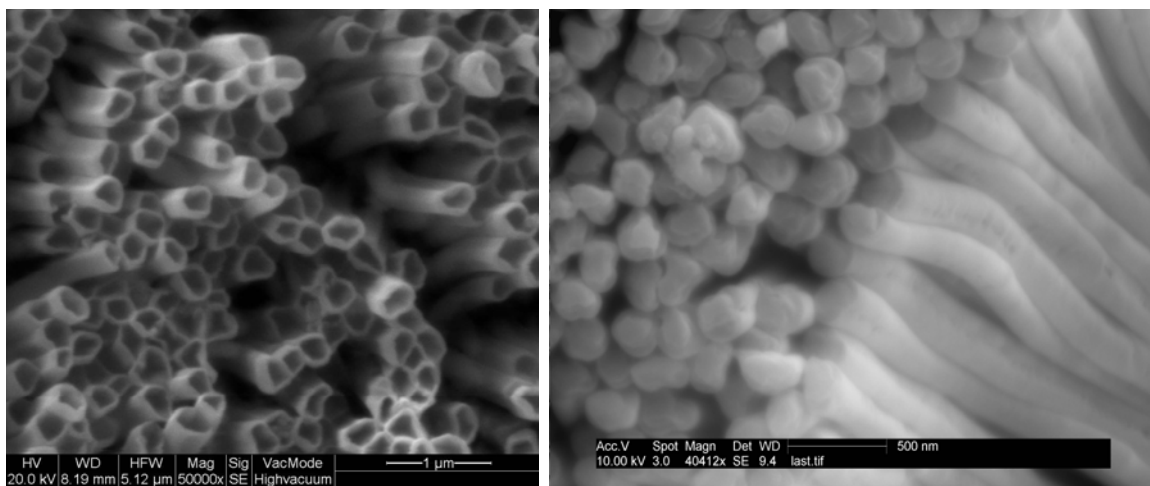


Figure 5.1(a, b). SEM top view of the PPy(DBS) nanowires. On the left (a), the hollow top portion of the nanowires can be clearly seen, on the right (b), the nanowires have been mechanically lapped.

thin sidewalls (< 20 nm), and probably unsuitable for mechanical actuation. To remove the hollow tube portion of the nanofiber, the following procedure was used: polypyrrole nanofibers of 40 μm length were electropolymerized in the alumina template as before, but before the alumina was dissolved, an extra step was added to the fabrication sequence. The alumina membrane with polypyrrole nanofibers was subjected to mechanical lapping to remove the top 10-15 μm of the nanofibers (Figure 5.2, Sample 1). The alumina was then dissolved in 0.2M NaOH (aq) solution, and the nanofibers imaged with an SEM. In Figure 5.1(b), it can be seen that the remaining lower portions of the nanofibers are solid, and therefore more suitable for actuation.

Therefore, it can be concluded that only the top few micrometers of the PPy(DBS) nanofibers were hollow.

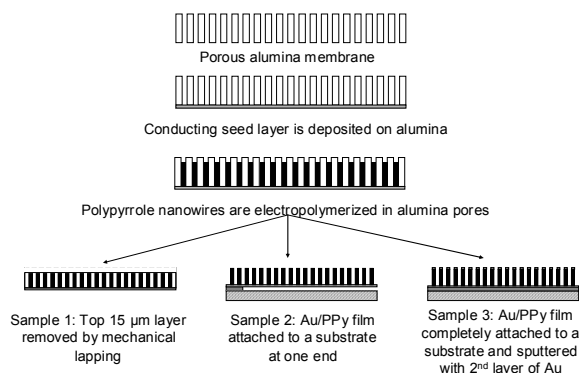


Figure 5.2. Schematic representation of the process flow, seen in cross section. Sample 1 was examined in a scanning electron microscope from top view, samples 2 and 3 were observed in cross section with an optical microscope.

5.2.2 SEM Evidence of Electrochemically Induced Volume Change in

Polypyrrole Nanowires. The ability of the polypyrrole nanowires to act as actuators was initially examined by SEM imaging. The nanowires were left embedded in the alumina membrane and then subjected to mechanical lapping to remove the top 10-15 μm (Figure 5.2, sample 1). The top surface was imaged with the scanning electron microscope (SEM) (Figure 5.3 A). As can be seen from the figure, the surface is smooth since the upper surfaces of the nanowires are even with the top surface of the alumina membrane. This assembly (lapped alumina membrane with embedded polypyrrole nanowires) was placed in the NaDBS electrolyte, with a platinum counter electrode and an Ag/AgCl reference electrode to complete the 3 electrode electrochemical cell. A voltage of -1 V versus the reference electrode was then applied between working and counter electrodes to induce reduction of polypyrrole

accompanied by the movement of sodium ions, which in turn resulted in expansion of nanowires. The membrane was then taken out of solution, dried, and imaged with SEM (Figure 5.3 B). The polypyrrole nanowires are clearly protruding from alumina surface as the result of ion influx and polymer swelling. Unfortunately, it is very hard to quantitatively evaluate the actuation with this method, since the sample has to be taken out of the electrochemical cell and dried to image the surface. However, it does provide clear qualitative evidence of nanowire actuation.[12]

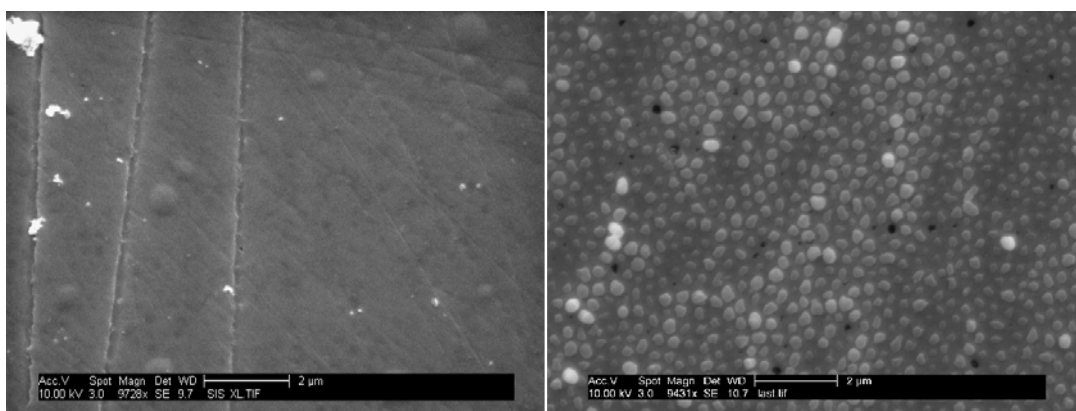


Figure 5.3. SEM image A shows the lapped and polished surface of alumina with top ends of PPy nanowires even with the surface; image B shows a similar sample after electrochemical reduction cycle in NaDBS electrolyte, with nanowires visibly expanding with the influx of sodium ions. Scale bars represent a distance of 2 μm .

5.2.3 Real Time Optical Microscopy of Nanowire Actuation. Two real time experiments were carried out using an optical microscope to detect reversible actuation of nanowires in both lateral and normal directions relative to electrode surface. First, we dissolved the alumina membrane, leaving a 5 mm x 5 mm gold film covered with PPy nanowires. The film was attached at one end to a substrate and mounted so that the cross section could be observed with an inverted optical microscope (Sample 2). The assembly was then immersed in electrolyte solution, and

electrodes were connected as before. Upon cycling the working electrode voltage between 0 and -1 V relative to the reference electrode, the composite film bent away and toward the substrate, respectively (Figure 5.4). Since PPy(DBS) contracts when oxidized (0 V) and expands when reduced (-1 V), the film's behavior is consistent with a bimorph interaction between polypyrrole nanowires and gold. This effect is somewhat surprising since nanowires are discrete; however, it seems that there is enough interaction between individual nanowires to behave similar to homogeneous polypyrrole films.

To detect whether the nanowires can also expand/contract in the direction normal to the gold film (along the nanowire length), the gold/polypyrrole nanowire film was completely attached to the substrate (Sample 3). A thin layer of gold was then sputtered on top of the polypyrrole nanowires to make optical measurement more precise. The substrate was subsequently sectioned and mounted such that the cross-section was visible in the microscope objective. The ends of the nanowires were clearly marked by the original gold seed layer on one side and the sputtered thin gold layer on the other (Figure 5.5 inset).

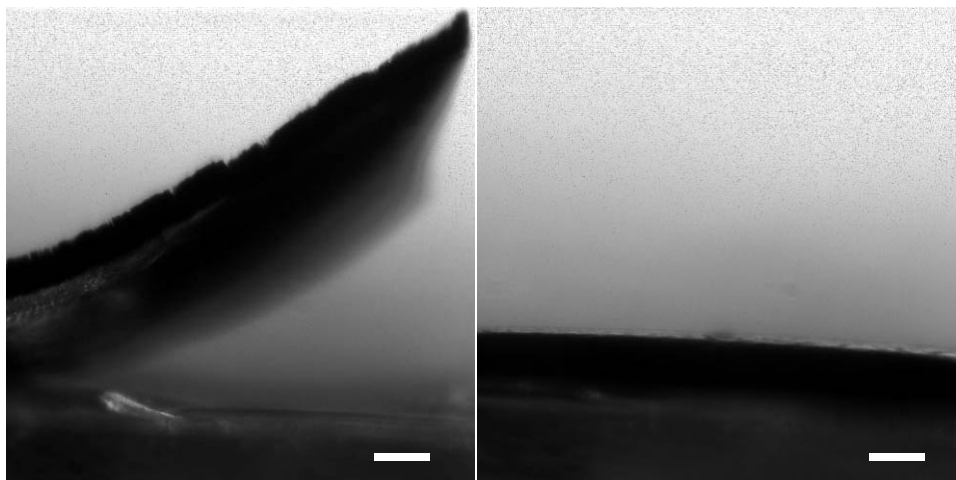


Figure 5.4. Micrograph A shows curving bimorph of polypyrrole nanowires (on top) and Au film (on the bottom). The bimorph was attached on the left to a substrate and polypyrrole was oxidized (V vs. Ag/AgCl = 0V) in NaDBS electrolyte, contracting the nanowires and curving the bimorph upward. Image B shows the same bimorph with swelled polypyrrole nanowires in an electrochemically reduced state (V vs. Ag/AgCl = -1 V). The scale bars represent 50 μm .

The actuation was carried out as above, and the opposing gold films were seen to move apart by $\sim 1.3 \mu\text{m}$ when the nanowires (43 μm long originally) were reduced at -1 V, and then move back to the original position upon oxidation at 0 V. The setup was put through > 20 cycles, and the magnitude of expansion/contraction remained the same. Cyclic voltammetry curve for the sample used in this experiment is shown in Figure 5.5, with prominent oxidation and reduction peaks.

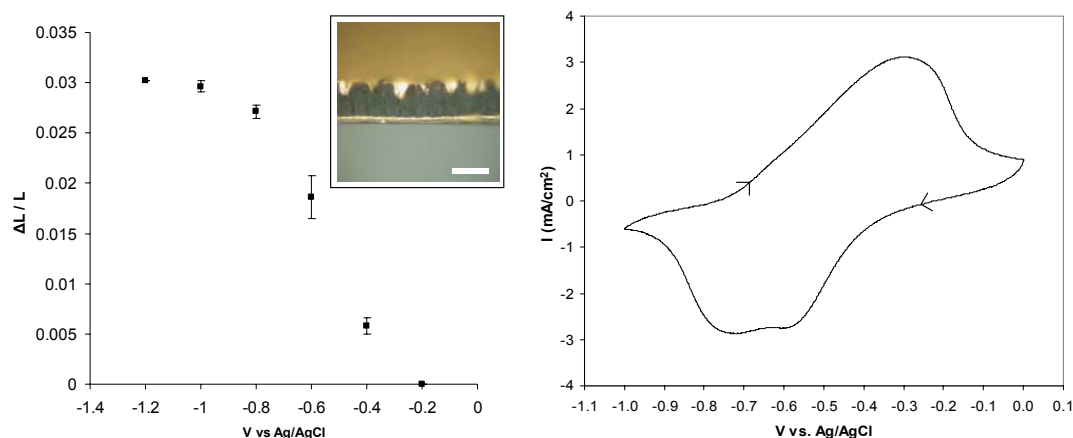


Figure 5.5. On the left, expansion of polypyrrole nanowires is shown as a function of voltage, starting with polypyrrole in an oxidized state and applying a voltage from -0.2 V to -1.2 V vs. the reference electrode. Original length of the nanowires $L = 43 \mu\text{m}$. The inset is an optical micrograph of the cross-section of the sample. The scale bar represents $50 \mu\text{m}$. On the right, a cyclic voltammetry of the same sample is shown, where an oxidation peak at -0.3 V and split reduction peaks at -0.61 V and -0.73 V can be seen.

5.2.4 Discussion of Optical Microscopy and Cyclic Voltammetry Data.

There is a strong correlation between the electrochemical behavior of the PPy nanowires and the observed length-wise expansion. When a negative voltage is applied to an oxidized PPy, it becomes chemically reduced and swells in size. However, the geometrical changes are not linear with voltage and can be explained by the cyclic voltammetry data. The reduction peaks occur after the voltage reaches -0.6 V, with the attendant increase in expansion at the same voltage. After -0.8 V, the expansion reaches its near maximum value, corresponding to a drop in current in the cyclic voltammetry curve as reduction of the nanowires is nearly complete. It was observed that the time response of the nanoactuators depended on their position in the sample. The nanowires at the edge tended to respond much faster than those in the middle of the sample, with response times (oxidation to reduction and back to

oxidized state) ranging from 2 seconds for the edge to more than 40 seconds for the middle of the sample (determined from measurements of current versus time). Since the response time is diffusion limited and defined by the position of a nanowire on the sample, we can conclude that the mass transport of sodium ions from the solution to the nanowires (as opposed to diffusion of ions inside the polypyrrole) and current density achieved at an individual nanowire are the limiting factors in our experiments. The switching speed of an isolated nanowire with no close neighbors is much faster than two seconds as the concentration of ions and the current density are maximized, and is examined below.

The PPy(DBS) nanowires retain actuation behavior of films prepared from the same material; however, some important changes can be seen. The vertical expansion (normal to electrode surface) of the films can be as high as 30% of the thickness of the film, but the same mode of expansion in nanowires produces displacements of only ~3% of nanowire length. It is not likely that this is due to the damage the nanowires sustained during dissolution of alumina, since the nanowires display very good electrochemical redox behavior. A more likely reason for this difference is that the PPy(DBS) nanowires don't retain the same internal morphology as the PPy(DBS) films. As was reported in the literature, polypyrrole films synthesized with surfactant dopants such as DBS⁻ display a columnar structure oriented perpendicular to the conducting seed substrate where the nucleation and subsequent growth of the polymer film starts.[13] In our case, a template of nano-sized pores causes the polymerization process to occur in a somewhat different manner. We mentioned in our previous

work[12] that the polymer nanowires appear as nanotubes when viewed from above with an SEM. We then removed the top portion of these 40 μm long nanowires by mechanical lapping to investigate whether the hollow center region extends to the conducting seed layer. It was found that only the top 1-2 μm portion is in fact a nanotube; the remaining length is a solid nanowire. This result suggests that the polymer growth starts both on the metal seed layer and on the pore walls, which is quite different from the case of a film which grows in only one direction. The difference in polymerization conditions induced by these very different geometries is likely the reason behind the different actuation performance of PPy(DBS) films and nanowires.

The expansion of nanowires in the lateral direction, or essentially the expansion of the nanowire diameter, could not be verified directly. It is likely that the bimorph behavior seen in Sample 2 is the summation of the lateral expansion with length-wise expansion, as some of the nanowires are not completely perpendicular to the gold surface.

5.3 POLYPYRROLE NANOWIRE MORPHOLOGY

Polypyrrole films doped with dodecylbenzenesulfonate undergo anisotropic volume change when undergoing electrochemical redox reactions. The anisotropy is significant: PPy(DBS) films undergo lateral length change (along the plane of the film) of 2-3%, while the thickness change (normal to the plane of the film) can be as

high as 30% [9]. The authors hypothesized that this can be attributed to an anisotropic morphology of the PPy(DBS) films. X-ray diffraction (XRD) data in the literature supports this hypothesis: polypyrrole films doped with n-alkylsulfonate ions have a strong scattering peak at low diffraction angles ($2^\circ < 2\theta < 5^\circ$) in addition to the broader diffraction peak at larger angles ($15^\circ < 2\theta < 25^\circ$) that is characteristic of the distance between pyrrole units in the polymer chains. The low angle peak is attributed to the presence of parallel planes that are normal to z-direction, or in-plane of the polymer film, and cause a Bragg reflection at an angle related to the spacing between the planes. It was found that the “lattice spacings” d are related to the size of the dopant ions according to the linear relationship:

$$d(n) = (0.19n + 1.2) \text{ nm},$$

where n is the number of carbon atoms in the hydrophobic tail of the n-alkylsulfonate dopant. This led authors to the conclusion that the morphology of the polypyrrole doped with large amphiphilic ions such as n-alkylsulfonates is that of alternating planes of polymer chains and dopant ions stacked tail to tail, and the interplane distance is related to the size of the dopant ion.[14] XRD results for chemically synthesized polypyrrole doped with dodecylbenzenesulfonic acid included a sharp peak at $2\theta = 3.34^\circ$ corresponding to d -spacing of 26.4 \AA [15], while XRD data for electropolymerized polypyrrole doped with different isomers of dodecylbenzenesulfonate was as follows: $d = 39.2 \text{ \AA}$ for PPy-(1D)BS, $d = 31.7 \text{ \AA}$ for PPy-(2D)BS, and $d = 24.2 \text{ \AA}$ for PPy-(6D)BS. [16]

The XRD data from the literature gives weight to the hypothesis that PPy(DBS) film morphology is strongly anisotropic, made up of alternating planes of polymer chains and dopant ions which lie in the plane of the film. The XRD reflection data from large area thick PPy(DBS) films on Au/Ti conducting seed layer electropolymerized in our laboratory is shown in Figure 5.6. A peak at $2\theta = 3.7^\circ$ is clearly visible, and corresponds to $d = 23.9 \text{ \AA}$ ($\lambda = 2d \sin \theta$, $\lambda = 1.54 \text{ \AA}$). This peak is

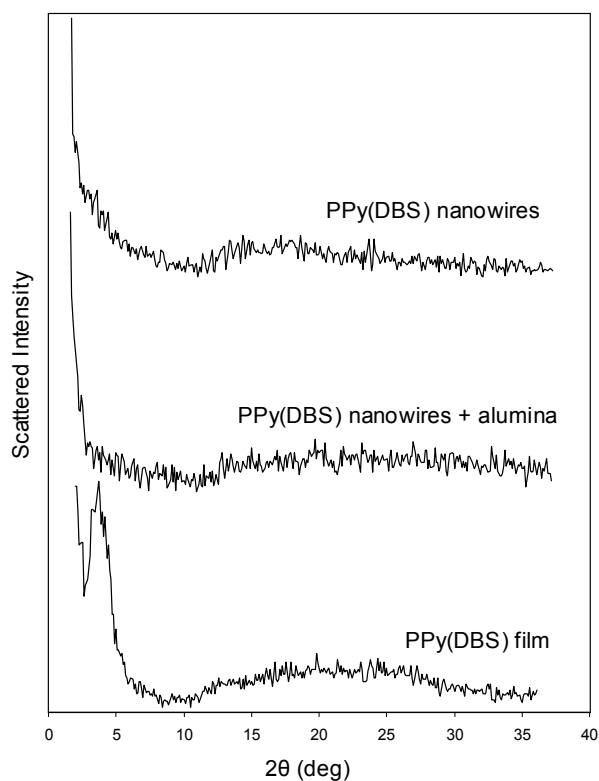


Figure 5.6 XRD data for large area PPy(DBS) film (50 μm thick), PPy(DBS) nanowires (50 μm long) embedded in alumina and with alumina removed.

somewhat broad, most likely due to the presence of different isomers in the dodecylbenzenesulfonate commercially available from Sigma-Aldrich, and is in agreement with the published data. It is likely that the anisotropy in the volume

change of polypyrrole film undergoing electrochemical redox is related to the morphological anisotropy, as the sodium ions and water molecules that enter the polymer matrix will tend to follow the layered structure of the film.

From the data shown in Figure 5.6 for PPy(DBS) nanowires it can be readily seen that the small angle peak is absent, while the broad diffraction due to pyrrole-pyrrole spacing is still present. Therefore, it must be concluded that the nanowires do not possess the layered plane structure in the z-direction (along the nanowire axis, or growth direction) that the PPy(DBS) films possess. The reason for this is not readily apparent, since the electropolymerization conditions were identical for both the film and the nanowires, but must be related to the nanoscale geometry. One possible cause involves surface interactions during polymerization between precipitating polypyrrole chains and the walls of the alumina pore, which disrupt the formation of the layered plane structure. Some evidence for this mechanism can be gathered from Figure 5.1(b), where the mechanical lapping of the top portion of the nanowires allows a look at the nanowire cross-section. It can be seen that the cross-section is not homogeneous, but consists of two phases – the circumference and the center region of the nanowire, supporting the assumption that surface interactions with the alumina pore walls affect nanowire morphology.

The internal morphology of the PPy(DBS) material has a strong effect on the anisotropy of the volume change and, therefore, on the magnitude of the volume change in a given direction. The reversible expansion of the polypyrrole films in lateral direction, where there is no alternating plane structure, is approximately 3% of

the original size. This is closely mirrored by 3% reversible length change of PPy(DBS) nanowires, which similarly lack layered plane structure in this direction as evidenced by x-ray diffraction experiments. It can be inferred from this data that the smaller-than-expected actuation magnitude of polypyrrole nanowires is due to the morphology change of polypyrrole when synthesized in nanowire geometry.

5.4 TIME RESPONSE OF ISOLATED NANOWIRES

5.4.1 Actuation speed in high-density nanowires. The speed of nanowire actuation, as observed with optical microscopy, varied depending on the position of the nanowires in the sample. Specifically, the nanowires at the edges of the sample responded significantly faster (2 seconds) than nanowires closer to the middle of the sample (30-40 seconds). The likely reason for the slower actuation is the impeded ion diffusion in the nanowires with close neighbors. As can be seen in the SEM images, the number of nanowires per unit area, or nanowire density, is quite high, and for the nanowire in the middle of the sample, the ion diffusion proceeds from top to bottom rather than from the nanowire wall to the center. Thus, the characteristic diffusion length is not 100 nm, the radius of the nanowire, but rather 43 μm , the nanowire length. The significantly longer ion diffusion slows down the actuation speed (and current response) of the nanowires, making the determination of true time constant of single nanowire difficult.

5.4.2 Fabrication of Isolated (Low-Density) Nanowires. In order to measure the time response of the nanowires unimpeded by negative effects of high density, a novel fabrication method was employed to increase the space between the nanowires. An alumina membrane with 20 nm pore size was used as a template for Au electrode electroplating (Figure 5.7).

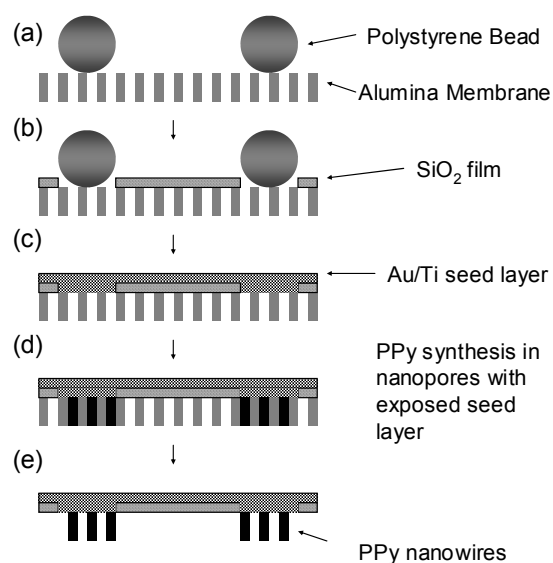


Figure 5.7 Fabrication sequence for electropolymerization of isolated polypyrrole nanowires

As the first step in the fabrication of electrodes, a suspension of 0.5 μm polystyrene beads in water was deposited onto the alumina membrane. The membrane was then air-dried, and a 50 nm film of SiO_2 was sputtered onto the side of the membrane with the microbeads. The beads were then removed by ultrasonication, followed by sputter-deposition of 10 nm Ti and 200 nm Au films to form a conductive seed layer for electroplating. The SiO_2 layer completely covered the 20 nm pores, preventing access of the electroplating solution to the seed layer below. On the other hand, the removal of the beads resulted in the exposed conducting layer in the bottom of some

of the pores – in this case, groups of pores with overall diameter of 500 nm (with 20 nm individual pores) and overall density of 1 group per 100 μm^2 . Polypyrrole nanowires were then electropolymerized in those pores where the gold conducting seed layer was exposed to the pyrrole monomer – NaDBS electrolyte solution. The alumina membrane was then dissolved in 0.5 M NaOH, and the resulting substrates held isolated groups of 40 μm long PPy(DBS) nanowires (Figure 5.8 A).

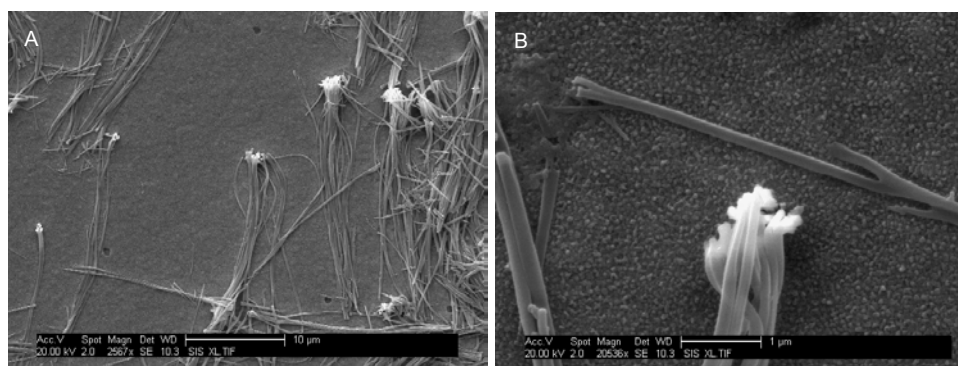


Figure 5.8 SEM images of the isolated PPy(DBS) nanowire groups. A: low magnification view; B: high magnification view of the nanowire attachment to Au conductive seed layer.

The nanowires appear to lie flat on the SiO_2 substrate in the SEM images due to the drying of the sample with the surface tension of evaporating water pulling nanowires down to the surface. However, as can be seen in Figure 5.8 (B), one end of the nanowires remains attached to the gold conductive layer underneath, thus providing the electrical connection for electrochemical experiments.

5.4.3 Experimental Results. Aside from reducing the density of nanowires per unit area, the fabrication methodology outline above has an important advantage of coating the conducting seed layer with an insulating film of SiO_2 in the areas with no nanowire growth. In subsequent electrochemical experiments, the double-layer

capacitance is therefore limited only to the nanowires. If the remaining area of Au conductive layer were left exposed to the solution, the current needed to charge up this large capacitor would be far larger than the current due to the electrochemical response of the nanowires, making experiments difficult to carry out.

The electrochemical characterization of isolated polypyrrole nanowires is shown in Figure 5.9.

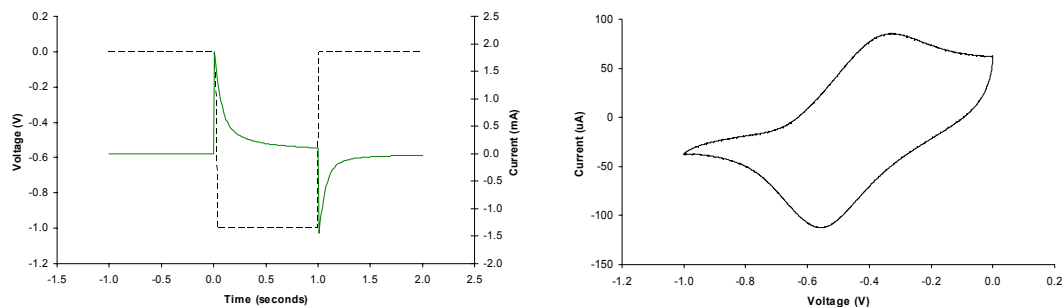


Figure 5.9 Electrochemical experiments on isolated nanowires. On the left, chronoamperometry, or current response (solid line) versus time to voltage steps (dashed line) is shown. On the right, cyclic voltammetry, or current response to a linear voltage ramp at 200 mV/sec is shown.

Well-defined characteristic oxidation and reduction peaks can be seen on the cyclic voltammetry graph (Figure 5.9, right), verifying that the current is indeed due to polypyrrole nanowires undergoing electrochemical redox reaction. The chronoamperometric curve (Figure 5.9, left) shows the time response of isolated polypyrrole nanowires. The current reaches 90% of its final value in 0.5 seconds or less, showing a significantly faster electrochemically controlled actuation compared to polypyrrole films or high density nanowires. In fact, this response time begins to approach the speed of biological nanoactuators such as skeletal muscle protein bundles.

5.4.4 Theory and Discussion. As discussed in chapter 2, there are several factors that determine the speed of actuation in polypyrrole devices. Two of the most important contributors to time delay seen between application of the voltage step and the completion of the electrochemically induced redox reactions in polypyrrole matrix are polymer chain conformational changes and the diffusion of dopant ions and water molecules [17]. The conformational changes play a role in opening up the polymer structure for subsequent diffusion, and are responsible for the current peak seen in chronoamperograms of polypyrrole films doped with small ions. In the case of polypyrrole doped with dodecylbenzenesulfonate, this peak is weak, visible only as an inflection in the doping chronoamperogram of PPy(DBS) thick films (Figure 2.6), but largely absent in chronoamperograms of both thin films and nanowires. Therefore, it seems reasonable to assume that diffusion, including the parallel diffusion of electronic charge, counterions and water [18], is the major factor affecting the time response of small-scale PPy(DBS) devices. Diffusion time depends heavily on the device geometry (shape and dimensions), and analytical expressions can be derived from Fick's Second Law of mass transport for simple geometries such as films and cylinders. The concentration-distance profile of concentrations (C) of undoped/doped polypyrrole in an infinite film of thickness l such that $0 < x < l$, where $x = l$ is the surface of the film that is exposed to solution, is given by [19]:

$$\frac{C - C_0}{C_1 - C_0} = 1 - \frac{4}{\pi} \sum_{n=0}^{\infty} \frac{(-1)^n}{2n+1} \exp \{ -D(2n+1)^2 \pi^2 t / 4l^2 \} \cos \frac{(2n+1)\pi x}{2l} \quad (5.1)$$

C_0 is the initial concentration, C_1 is the maximum concentration of counterions and water in the film, and D is the effective diffusion coefficient for simultaneous transport of electronic charge, counterions and water. In a cylinder of radius a such that $0 < r < a$, where $r = a$ is the cylinder surface exposed to solution, the concentration profile is given by the following:

$$\frac{C - C_0}{C_1 - C_0} = 1 - \frac{4}{a} \sum_{n=1}^{\infty} \frac{\exp(-D\alpha_n^2 t) J_0(r\alpha_n)}{\alpha_n J_1(a\alpha_n)} \quad (5.2)$$

J_0 and J_1 are Bessel functions of orders zero and 1, respectively, where $a\alpha_n$ are the roots of the Bessel function of the first kind of order zero.

The concentration profiles given in equations (5.1) and (5.2) are plotted in Figure 5.10. The current due to the concentration gradient can be determined by multiplying $\partial C / \partial x$ ($x = l$) by $nFAD$, where A is the effective area [20]:

$$i_{(l,t)} = \frac{nFAD^{1/2}C_0}{\pi^{1/2}l^{1/2}} \times \sum_{k=0}^{\infty} (-1)^k \left[\exp\left(-\frac{k^2 l^2}{Dt}\right) - \exp\left(-\frac{(k+1)^2 l^2}{Dt}\right) \right] \quad (5.3)$$

The normalized currents for both planar and cylindrical geometries are plotted in Figure 5.11. It can be seen from the plot that for equal characteristic dimensions, $l = a$, the current in a cylinder decays faster than in the plane, due to the more concentrated diffusion flux lines in the cylinder. Furthermore, the characteristic current decay time, signifying the completion of the doping or undoping process in the polymer, is directly proportional to the square of the characteristic dimension (thickness in a film and radius in a cylinder). Therefore, polypyrrole devices with

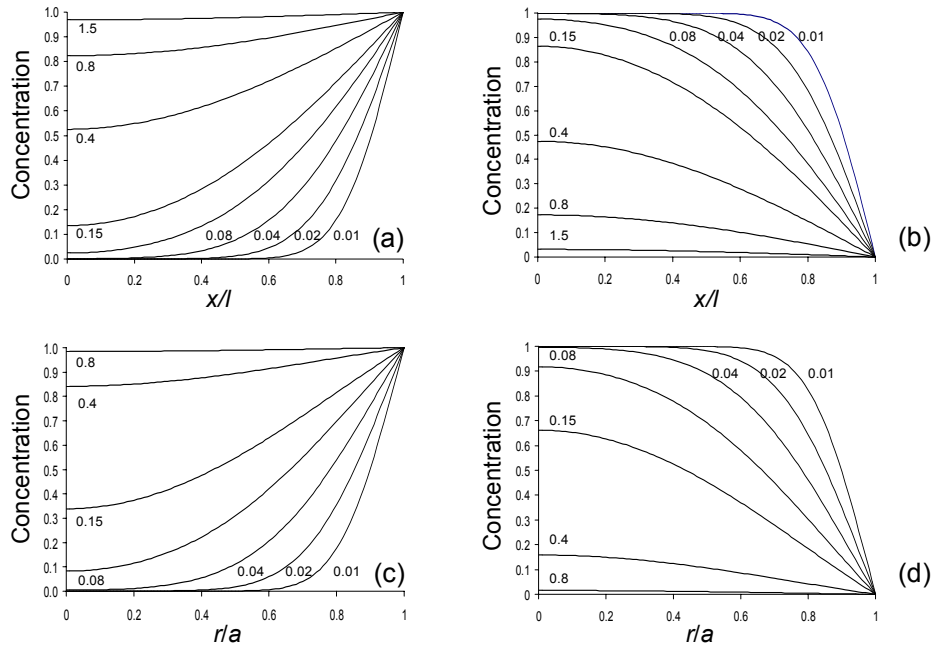


Figure 5.10 Concentration profile versus distance at various times. The numbers on the curves are values of Dt/l^2 in (a) and (b), and Dt/a^2 in (c) and (d). A film of thickness l is undergoing reduction, with ions moving into the film from surface $x = l$ in (a), while (b) is the plot of the concentration profile during oxidation (ion and water movement out of the film) in a film. The same processes are plotted for a cylinder of radius a in (c) and (d).

small nanoscale dimensions are significantly faster than macro- and even micro-scale actuators. This conclusion is supported by experimental evidence as reported above, with the characteristic time of the electrochemical reactions in nanowires with $r = 100$ nm below 0.5 seconds.

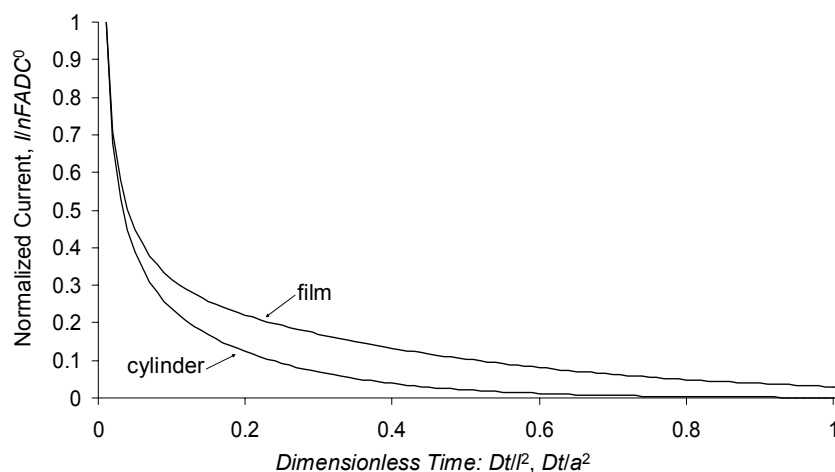


Figure 5.11 Diffusion-controlled current plotted versus dimensionless time, Dt/l^2 in a planar geometry, and Dt/a^2 in a cylinder.

Since the linear expansion of polypyrrole nanowires is only $\sim 3\%$, a useful nanoactuator can be made by forming a bilayer structure involving a single nanowire attached to a parallel layer or nanowire of a different material. Bilayer structures are commonly used to amplify a small change in volume to a large angular movement by generating a stress gradient across the interface between the polymer and the secondary material. For example, polypyrrole-gold micro-bilayers have been utilized to convert 0.5-3% of linear motion into 180 degrees or more of angular motion.[8] An analogous structure can potentially be produced at nanoscale dimensions, namely a bilayer structure amplifying the motion of a single polypyrrole nanowire and capable of performing tasks such as nano-particle manipulation and cilia-like motion.

5.5 CONCLUSION

In conclusion, it was demonstrated that template synthesis of conducting polymer nanowires can be used to produce electrically controlled nanoactuators operating in an aqueous electrolyte. The nanowires expanded/contracted by approximately 3% of their original length under applied voltage; however, coupling of nanowire geometrical changes with gold (or other materials) in a bimorph structure can be used to amplify the magnitude of actuation significantly. Since the electrochemical actuation requires only the presence of small positively charged ions in the fluid, these nanoactuators are suitable for operation in a wide variety of environments such as blood plasma or salt water with potential applications in micro and nanofluidics for medicine, biosciences, and environmental monitoring.

5.6 APPENDIX: Experimental Details.

Alumina membranes (Whitman) with 0.2 μm pore size were used as received. The seed gold layer was fabricated as follows: first, 100 nm Au was sputtered onto one surface of the membrane, then, a 1.5 μm layer of Au was electroplated onto the Au thin film to seal the pores. Electropolymerization was carried out in a solution of 0.1 M pyrrole, 0.1 M NaDBS at 0.55 V vs. Ag/AgCl reference with a Pt mesh counter electrode using a Gamry PCI4-300 potentiostat. Sample 1 was mechanically lapped to remove the top 10-15 μm of alumina and embedded nanowires by using a 3 stage

manual process with polishing films of 9 μm , 1 μm , and 0.3 μm aluminum oxide grit (Fiber Instrument Sales, Inc.). Actuation was performed in 0.1M NaDBS (aq) with the same reference and counter electrodes connected to the potentiostat. Sample 3 was coated with 350 nm Au sputtered film to aid optical visualization, and mounted by compressing against a thin layer of thermal wax on a glass cover slip. Images were captured on an optical microscope with a digital video CCD camera and analyzed with Metavue (Universal Imaging Corp.) software. Expansion data shown in Figure 5.5 represents averages of 4 measurements for each voltage value taken at different areas of the same sample. X-ray experiments were carried out on a double crystal diffractometer. Samples were mounted with lead tape to a glass slide, which was in turn mounted on an aluminum sample holder of the diffractometer. Angle θ was measured between the scattered beam and the plane of the sample, with the z-direction normal to the plane of the sample. For both film and nanowire samples, z-direction corresponded to the growth direction of the polypyrrole during electropolymerization. Diffraction of nanowires was taken with alumina intact, to ensure that the nanowires were parallel to the z-axis, and with alumina dissolved to verify that diffraction from Al_2O_3 introduced no artifacts into the measurement of scattered intensity.

5.7 ACKNOWLEDGEMENTS

This research was supported by funding under AFOSR MURI program. The text of Chapter 5 is, in part, a reprint of the material as it appears in Y. Berdichevsky,

and Y.-H. Lo, *Mater. Res. Soc. Symp. Proc.* Vol. 872, J13.4.1-J13.4.5, 2005, and *Advanced Materials* 18, 122-125, 2006. The dissertation author was the primary researcher and author and the co-author listed in these publications directed and supervised the research which forms the basis of this chapter.

5.8 REFERENCES

1. A. M. Fennimore, T. D. Yuzvinsky, W.-Q. Han, M. S. Fuhrer, J. Cumings and A. Zettl, "Rotational actuators based on carbon nanotubes," *Nature* 2003, 424, 408.
2. H. G. Craighead, "Nanoelectromechanical Systems," *Science* 2000, 290, 1532.
3. A. Requicha, "Nanorobots, NEMS, and Nanoassembly," *Proceedings of the IEEE* 2003, 91, 1922.
4. T. F. Otero and J. M. Sansiñena, "Artificial muscles based on conducting polymers," *Bioelectrochem. Bioen.* 1995, 38, 411.
5. R. H. Baughman, "Conducting polymer artificial muscles," *Synthetic Metals* 1996, 78, 339.
6. C. R. Martin, "Template Synthesis of Electronically Conductive Polymer Nanostructures," *Acc. Chem. Res.* 1995, 28, 61.
7. Q. Pei and O. Inganäs, "Electrochemical applications of the bending beam method .2. Electroshrinking and slow relaxation in polypyrrole," *J. Phys. Chem.* 1993, 97, 6034.
8. E. Smela, "Microfabrication of PPy microactuators and other conjugated polymer devices," *J. Micromech. Microeng.* 1999, 9, 1.
9. E. Smela and N. Gadegaard, "Volume change in polypyrrole studied by atomic force microscopy," *J. Phys. Chem. B* 2001, 105, 9395; "Surprising volume change in PPy(DBS): An atomic force microscopy study," *Adv. Mater.* 1999, 11, 953.
10. Y. Berdichevsky and Y. -H. Lo, "Polymer Microvalve Based on Anisotropic Expansion of Polypyrrole," *Mat. Res. Soc. Symp. Proc.* 2004, 782, A4.4.1.

11. Y. Berdichevsky and Y. -H. Lo, "Fabrication of Polypyrrole Nanowires," *Proc. SPIE* 2005, 5759, 268.
12. Y. Berdichevsky and Y. -H. Lo, "Fabrication and Evaluation of Conducting Polymer Nanowire Heterostructures," *Mat. Res. Soc. Symp. Proc.* 2005, 872, J13.4.1.
13. K. Naoi, Y. Oura, M. Maeda and S. Nakamura, "Electrochemistry of surfactant-doped polypyrrole film(I) – formation of columnar structure by electropolymerization," *J. Electrochem. Soc.* 1995, 142, 417.
14. W. Wernet, M. Monkenbusch, and G. Wegner, "A new series of conducting polymers with layered structure: Polypyrrole n-alkylsulfates and n-alkylsulfonates," *Makromol. Chem., Rapid Commun.* 5, 157-164, 1984.
15. M.-K. Song, Y.-T. Kim, B.-S. Kim, J. Kim, K. Char, and H.-W. Rhee, "Synthesis and characterization of soluble polypyrrole doped with alkylbenzenesulfonic acids," *Synthetic Metals* 141, 315-319, 2004.
16. K. West, L. Bay, M. M. Nielsen, Y. Velmurugu, and S. Skaarup, "Electronic Conductivity of Polypyrrole-Dodecyl Benzene Sulfonate Complexes," *J. Phys. Chem. B* 108, 15001-15008, 2004.
17. T. F. Otero, H.-J. Grande, and J. Rodriguez, "Reinterpretation of Polypyrrole Electrochemistry after Consideration of Conformational Relaxation Processes," *J. Phys. Chem. B*, 101, 3688-3697, 1997.
18. P. Daum, J. R. Lenhard, D. Rolison, and R. W. Murray, "Diffusional Charge Transport through Ultrathin Films of Radiofrequency Plasma Polymerized Vinylferrocene at Low Temperature", *J. Am. Chem. Soc.* 102, 4649-4653, 1980.
19. J. Crank, "The Mathematics of Diffusion," Clarendon Press, Oxford, UK, 1975.
20. D. M. Oglesby, S. H. Omang, and C. N. Reilley, "Thin Layer Electrochemical Studies Using Controlled Potential or Controlled Current," *Anal. Chem.* 37, 1312-1316, 1965.

CHAPTER 6

Template-fabricated Nanoscale Biosensors for Catecholamine Detection

6.1 INTRODUCTION

Electrochemical methods for the detection of neurotransmitters such as dopamine and norepinephrine can provide valuable information about the function of mammalian central nervous system and are used both *in vivo* and *in vitro* [1, 2]. Typically, such detection schemes utilize a carbon microelectrode to sample neurotransmitter release in different regions of the brain or a brain slice, with or without external stimulation. The concentration of catecholamine neurotransmitters dopamine and norepinephrine is measured by applying a potential at the electrode and measuring the anodic current that results from oxidation of the catecholamine molecules. Ideally, detection is carried out in real time to record the variation in concentration due to release and subsequent uptake of neurotransmitters. A variety of electrochemical techniques such as cyclic voltammetry and differential pulse voltammetry are used to provide specificity to the detection by discriminating between the electrochemical behavior of a variety of oxidizable molecules in the extracellular fluid. However, such voltammetric methods require scanning through a range of different voltages to record the current, and take more time than simple constant potential amperometry. In order to enable the use of these techniques to measure real time changes in neurotransmitter concentration, fast electrode response is required [3]. It was found that by decreasing the size of the electrodes, improved mass transport and decreased double layer capacitance can be achieved, resulting in an increase in signal-to-noise ratio and a better time response [4, 5]. In this work, we demonstrate

nanoelectrodes fabricated without the requirement of nanolithography that have a faster time response compared to microelectrodes while maintaining excellent sensitivity to dopamine.

An interesting application of electrochemical detection of neurotransmitters involves using the electrodes on a brain slice *in vitro*, allowing precise positioning of stimulation and detection electrodes in a controlled environment where the brain region of interest can be easily observed with an optical microscope. However, current microelectrode design requires fabrication of one electrode at a time, which then needs to be positioned relative to the slice with the help of micrometers. In this work, nano-sized electrodes are integrated with an insulated substrate suitable for placement of brain slices, allowing the detection of catecholamine release over large area while maintaining a small electrode size and fast time response.

6.2 EXPERIMENT

Template synthesis of gold (Au) and conducting polymer nanostructures using template synthesis techniques has been reported previously [6], and was adopted here with an addition of a masking step to reduce the density of deposited nanostructures. An alumina membrane with 20 nm pore size was used as a template for Au electrode electroplating (Figure 6.1).

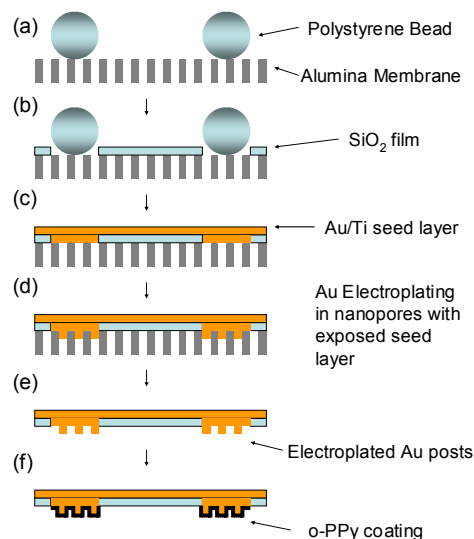


Figure 6.1 Fabrication sequence for making nanoelectrodes: (a) polystyrene bead suspension is deposited onto an alumina membrane; (b) SiO₂ film is deposited by ion sputtering; (c) beads are removed by ultrasonication, and Ti/Au seed layer is sputtered onto the substrate; (d) gold is electroplated through the alumina pores where the seed layer is exposed to solution; (e) alumina membrane is dissolved.

As the first step in the fabrication of electrodes, a suspension of 0.5 μm polystyrene beads in water was deposited onto the alumina membrane. The membrane was then air-dried, and a 50 nm film of SiO₂ was sputtered onto the side of the membrane with the microbeads. The beads were then removed by ultrasonication (Figure 6.2 (b)), followed by sputter-deposition of 10 nm Ti and 200 nm Au films to form a conductive seed layer for electroplating. The SiO₂ layer completely covered the 20 nm pores, preventing access of the electroplating solution to the seed layer below. On the other hand, the removal of the beads resulted in the exposed conducting layer in the bottom of some of the pores – in this case, groups of pores with overall diameter of 500 nm (with 20 nm individual pores) and overall density of 1 group per 100 μm^2 . The structure is completed by short Au electroplating, creating Au posts of approximately

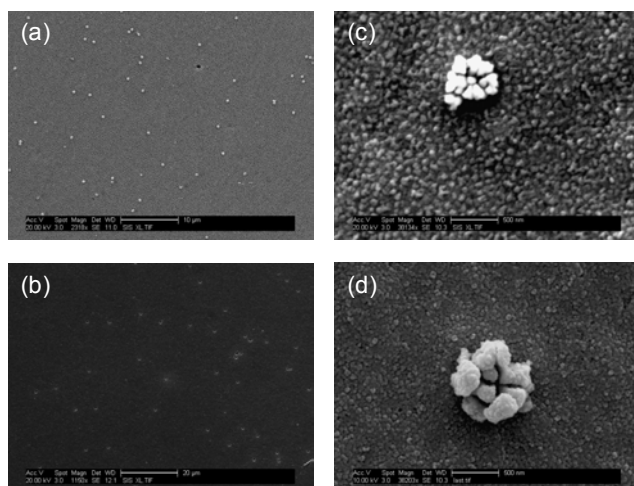


Figure 6.2 Scanning electron microscope (SEM) images at different fabrication steps: (a) polystyrene microbeads dispersed on the alumina membrane; (b) openings in the oxide film after the beads have been removed; (c) single electrode composed of a group of electroplated Au nanoposts; (d) the electrode with the deposited o-PPy coating.

50 nm height, followed by dissolution of the alumina membrane in 0.5 M sodium hydroxide. Each 500 nm group of 20 nm Au posts (Figure 6.2 (c)) is an electrode with large surface area. By varying the size of the beads and the concentration of the beads in the suspension when deposited onto the alumina membrane, the configuration of the electrodes can be controlled both in terms of overall diameter and the density of the electrodes on the substrate. In this work, the nanostructured electrodes are connected with each other, allowing the recording of a single signal from a large area. However, in applications requiring parallel recording from small areas of a brain slice, the Ti/Au seed layer can be micropatterned to allow multiple electrical connections.

In order to provide selectivity in detection, particularly when a large concentration of other oxidizable molecules such as ascorbic acid (AA) is present in the solution, the electrodes were coated with a thin film of overoxidized polypyrrole (o-PPy), which is a positively charged conducting polymer that rejects ascorbate

anions at physiological pH [7]. Briefly, polypyrrole was electropolymerized on the electrode in a solution of 50 mM pyrrole monomer and 0.2M KCl by cycling six times between the potentials of 0 and 1.1 V at a sweep rate of 500 mV s^{-1} . The overoxidation was then performed by cycling between the same potentials in 0.5 M NaOH until polypyrrole was no longer electroactive. Nanostructured electrode with o-PPy coating is shown in Figure 6.2(d).

The electrodes were tested in a phosphate buffered solution (pH 7.4) with a $100 \text{ }\mu\text{M}$ ascorbic acid background to simulate physiological conditions. Electrodes were kept at a constant anodic potential (0.5 V) and the change in current was monitored while small concentrations of dopamine were sequentially added to the solution. Arrows in Figure 6.3 correspond to an addition of a defined concentration of dopamine to the solution (25 nM, 50 nM, 100 nM), causing a corresponding step in the current. The size of the current step is plotted against the increase in concentration in the inset in Figure 6.3. There is a linear relationship between changes in concentration and current, demonstrating the suitability of nanoelectrodes for taking quantitative measurements of changing dopamine levels against an ascorbic acid background with more than a thousand times higher concentration than that of dopamine.

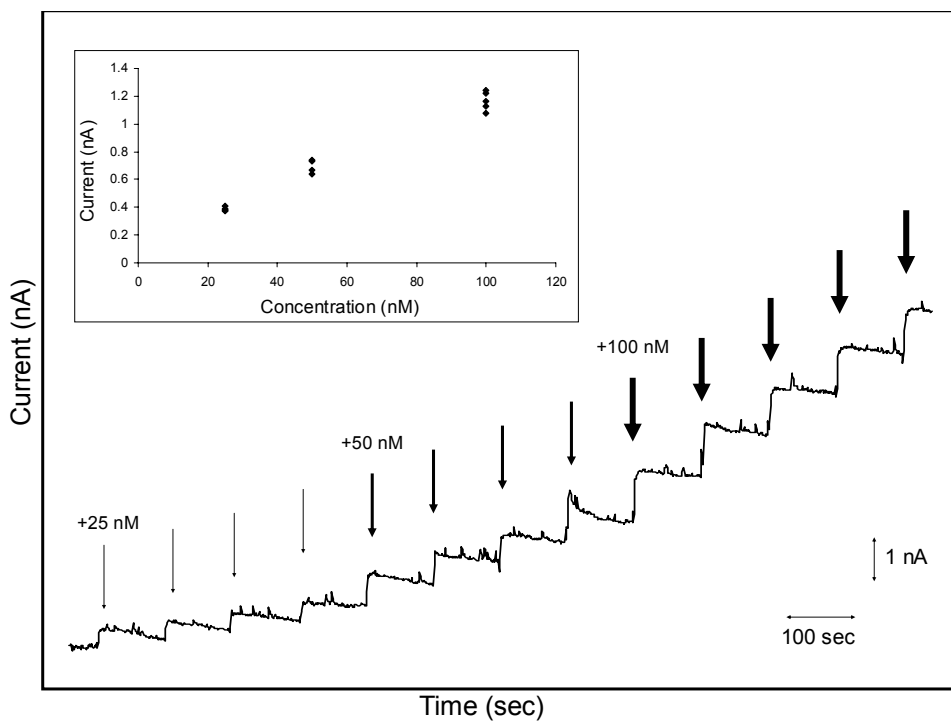


Figure 6.3 Current response due to addition of small concentrations of dopamine. Thin arrows represent additions of 25 nM of dopamine to solution, medium arrows 50 nM additions, and thick arrows 100 nM addition of dopamine. The inset shows the change in current when a defined concentration of dopamine is added.

6.3 DISCUSSION

In addition to current measurements at a constant potential, a variety of other voltammetric techniques can be used for the detection of electrochemically oxidizable species of interest. One such technique is differential pulse voltammetry (DPV), where the applied potential consists of a voltage ramp with superimposed small amplitude potential pulses. The current is measured before each pulse, and is subtracted from the current value at the end of the pulse. The recorded current is therefore in differential form, plotted against a voltage range. Different chemical

species oxidize at slightly different voltages, resulting in current peaks centered at a characteristic voltage value for each molecule and providing more specific detection than amperometry. Furthermore, DPV keeps the residual current (due to the charging of double layer capacitance) low, increasing the sensitivity. An accumulation step can be used with DPV, pre-concentrating the analyte at the electrode surface prior to applying oxidizing potential, which also results in an improvement in sensitivity. Unfortunately, the increased sensitivity is accomplished at the expense of time resolution, as the voltage scan requires about 80 seconds (1), while the pre-concentration step takes another 100 seconds (3) to achieve the sensitivity required for measuring dopamine levels as low as 5 nM. This makes real time experiments measuring dopamine release due to external stimulation very difficult. Therefore, electrodes with a faster time response (due to decreased size as discussed above) can be particularly suitable for scanning voltammetric techniques such DPV or differential pulse stripping voltammetry (DPSV, or DPV with the added accumulation step). In Figure 6.4, the nanoelectrode DPSV scan of 2.5 nM dopamine in PBS solution is shown, with the background current digitally subtracted. The accumulation time was reduced to only 5 seconds, but the dopamine peak is still clearly visible. This shows that nanoelectrodes with improved time response can have an important role to play in speeding up the voltage scan times used with the high-sensitivity voltammetric techniques.

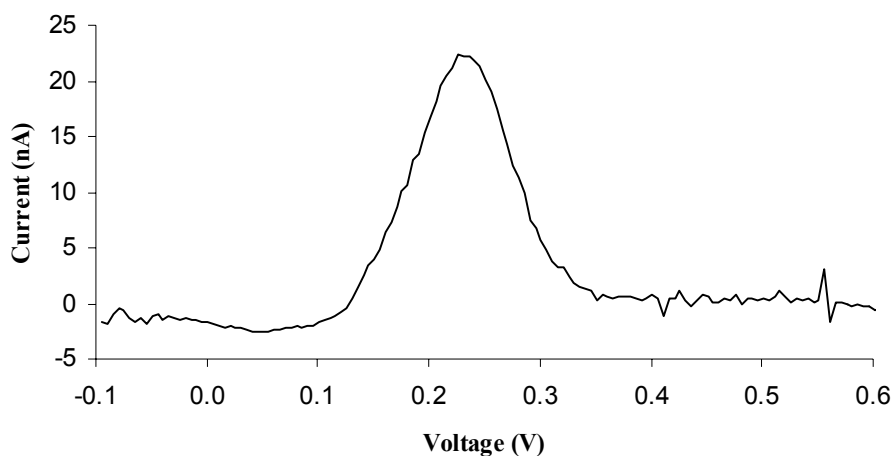


Figure 6.4 Differential pulse stripping voltammetry of 2.5 nM dopamine in PBS solution. The current is shown with the background digitally subtracted, and the dopamine peak is clearly visible.

6.4 CONCLUSION

In conclusion, novel nanostructured electrodes were fabricated for electrochemical sensing of catecholamine neurotransmitters such as dopamine. The electrodes demonstrated improved time response, particularly with voltammetric techniques requiring voltage scans, while detecting nanomolar concentrations of dopamine. The nanoelectrodes had a linear response to changing dopamine concentration in the presence of high background, enabling quantitative and high-sensitivity determination of dopamine levels in physiological conditions.

6.5 ACKNOWLEDGEMENTS

This work was supported by funding for AFOSR MURI program. The author would also like to thank Kai Zhao for valuable discussion and input.

6.6 REFERENCES

- (1) Kawagoe K. T.; Zimmerman J. B.; Wightman R. M.; *J Neurosci Meth* **1993**, 48, 225-240.
- (2) Stamford J. A.; Justice, Jr J. B.; *Anal Chem* **1996**, 68, 359-366.
- (3) Zhang, X.; Ogorevc, B.; Tavcar G.; Svegli I. G.; *The Analyst* **1996**, 121, 1817-1822.
- (4) *Ultramicroelectrodes*, ed. Fleischmann, M.; Pons, S.; Relison, D. R.; Schmidt, P.P.; Datadech Systems, Morgantown, 1987.
- (5) Tanaka, K.; Kashiwagi, N.; *J. Electroanal. Chem.* **1989**, 275, 95.
- (6) C. R. Martin, *Acc. Chem. Res.* **1995**, 28, 61.
- (7) Olivia, H.; Sarada, B. V.; Shin, D.; Rao, T. N.; Fujishima, A.; *The Analyst* **2002**, 127, 1572-1575.

APPENDIX

Experimental Details of Nanowire Fabrication and SEM images

Nanowire actuators and nanosensors described in Chapters 5 and 6 were fabricated using commercially available porous alumina membranes as templates. In the description that follows below, the reasoning behind the choice of the membrane for a particular experiment, and modification of the membranes with microbeads and oxide deposition, is explained with accompanying SEM images to illustrate different stages of the fabrication.

Membranes used in the work were 13 mm Anodisc filters purchased from Fisher Scientific. A membrane with a nominal pore diameter of 200 nm, used for fabrication of “high-density” per area PPy nanowires, has structure shown in the SEM images in Figure A.1. The distribution of the pores can be seen in Fig. A.1(B): the pores are not completely cylindrical, have somewhat varying diameters, and are randomly distributed with high density (approaching 50% of the surface area of the membrane). From the cross-section images of Fig A.1(A) and A.1(C), it can be noted that the pores go all the way through the membrane, make an angle of 90° with the membrane surfaces, and are isolated from each other. Some care must be taken in the analysis of the cross-section images of the alumina membranes since the membranes are not crystalline and the line along which the membranes were sectioned does not necessarily go through the widest portion of the pores. Therefore, the apparent differences in pore diameters visible in Fig. A.1(C) are not representative of the actual pore size distribution.

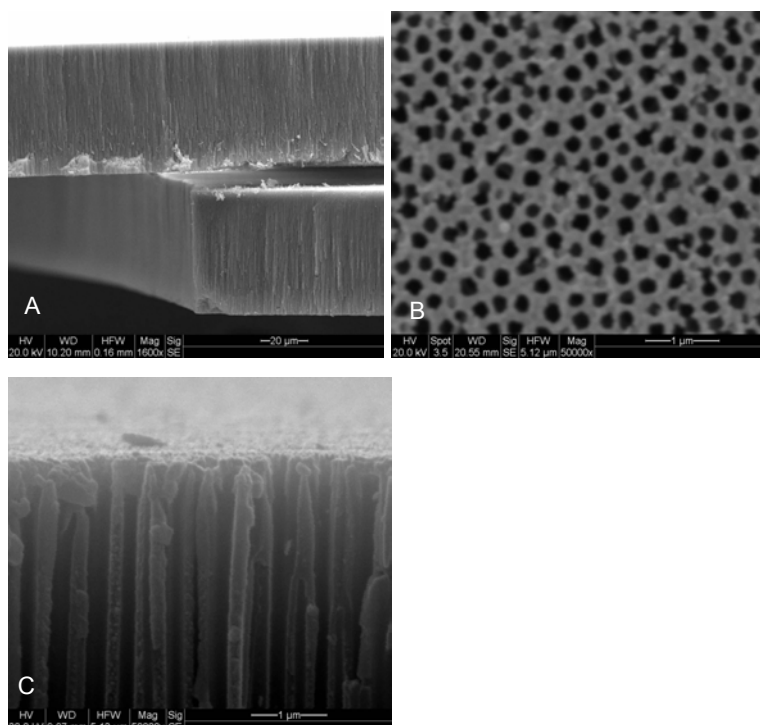


Figure A.1 A, cross-section of 200 nm alumina membrane; B, top-view of the same membrane showing pore distribution; C, close up of the cross-section of the pores.

The pore density in a commercially available alumina membrane is very high: if the membrane is used as is, the density of the template-synthesized nanostructures will mirror that of the membrane. In some applications, particularly high-speed nanowire actuators and nanosensors, it is desirable to reduce the density of active pores, as described in Chapters 5 and 6, while still using the commercially available alumina membranes (which are convenient, in terms of their easy availability, long-pore length, and rigidity that allows additional planar fabrication steps). The process methodology was schematically described earlier, and involves placement of the microbeads onto alumina surface to act as a shadow mask for the sputtered silicon dioxide film which deactivates some of the pores. This process was first tried on the 200 nm pore

diameter membranes. The polystyrene microbeads of 0.5 μm diameter were suspended in a water solution at a known concentration, and micropipetted onto an alumina membrane. The water was either allowed to air-dry, or was absorbed into a lint-free paper filter placed underneath the alumina disk. The resulting bead distribution on alumina surface depends on the concentration of beads in suspension, while the method used to dry the membranes had an effect on the homogeneity of the bead distribution. Allowing the water to air-dry tended to pull the beads together due to water surface tension, creating regions of low and high bead density. Some of the bead distributions are shown in the SEM images in Figure A.2.

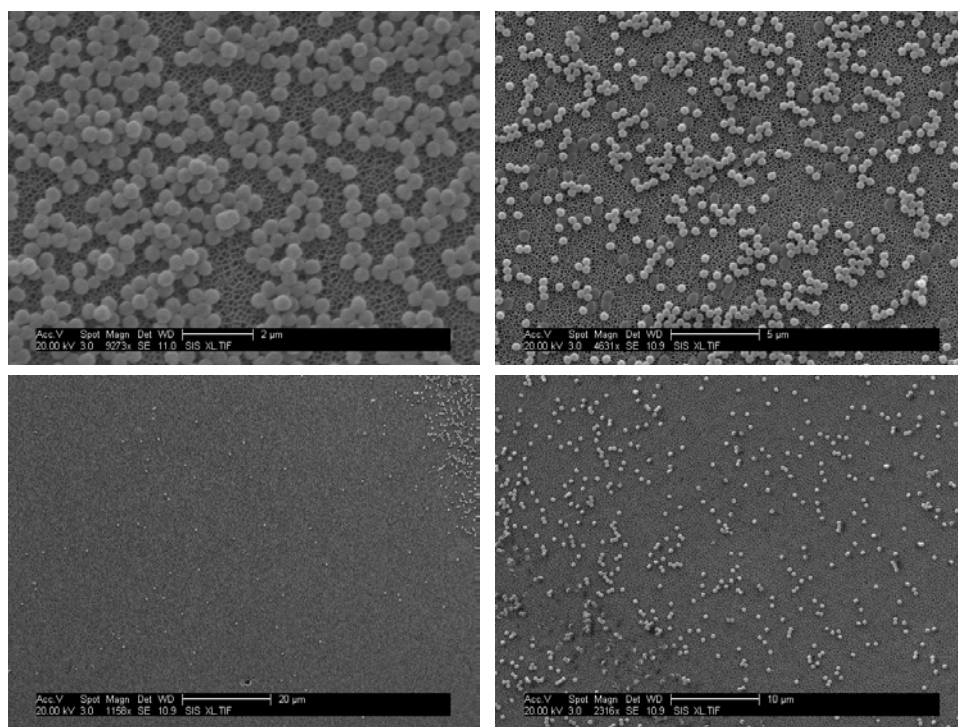


Figure A.2 Polystyrene microbeads on alumina surface, with varying bead suspension concentrations.

Sputtered SiO_2 film was used to render some of the pores inactive, to act as an insulator between the subsequently deposited metal film and the

electroplating/electropolymerization solution. In order to completely cover the pores, the SiO_2 film needed to be at least 200 nm thick, and deposited at an elevated temperature with concurrent ion etch to ensure conformal coating. In the Denton Sputtering system, the following parameters were used: RF power of 350 W, stage rotation of 60, stage temperature at 40° C, and RF stage bias (concurrent etch) of 40 W. The deposition rate was determined to be approximately 2.5 nm / minute. The SEM images of the alumina/bead substrate with 300 nm SiO_2 coating are shown in Figure A.3.

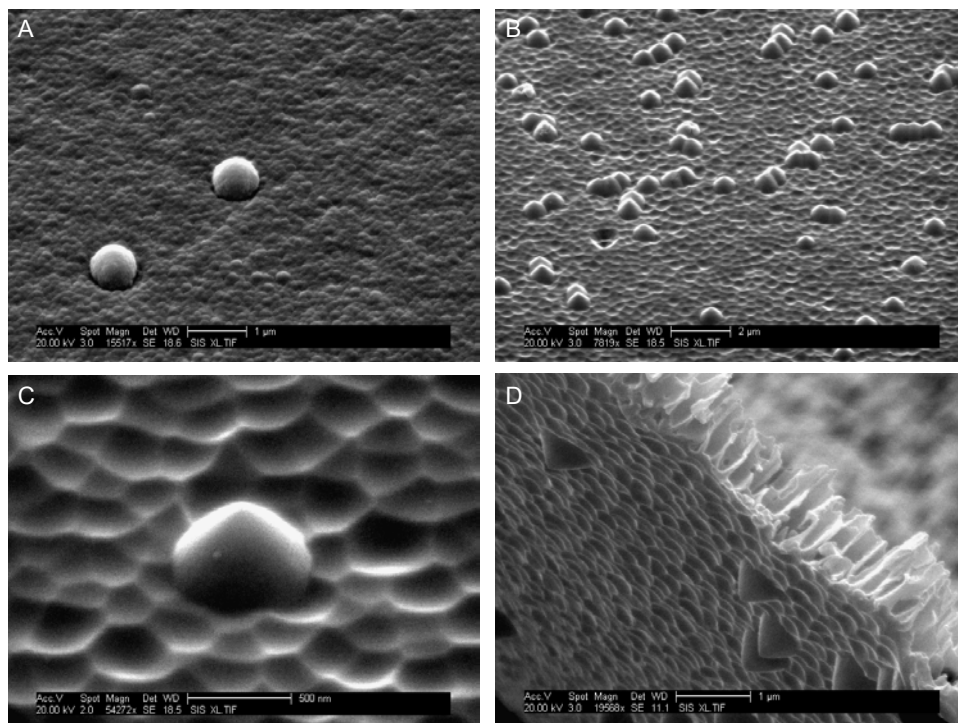


Figure A.3 Sputtering of 300 nm SiO_2 film onto alumina/bead substrate. A, SiO_2 film sputtered without concurrent substrate etch; B, with substrate etch; C, close-up of a single SiO_2 coated bead after ultrasonication; D, after removing alumina in NaOH, SiO_2 penetration into the pores becomes visible.

In Figure A.3(A), SiO_2 film was deposited without the concurrent RF bias applied to the sample stage, resulting in a very rough film structure. This film did not seal the

pores completely, allowing the electrolyte to leak through. A much smoother film surface can be seen in Figure A.3(B), where the film was sputtered with the RF stage bias. However, the unfortunate side effect of the improved conformity of 300 nm SiO₂ coating was the permanent sealing of the microbeads to alumina surface, with the ultrasonication step no longer capable of removing the beads (Figure A.3(C)).

Another issue with sputtering 300 nm of silicon dioxide on a membrane with 200 nm pores is the deep (up to 1 μ m) penetration of SiO₂ into the pores, resulting in a structure shown in Figure A.3(D) after the removal of the alumina in 0.5 M NaOH.

In order to address these problems, an alumina membrane with the nominal diameter of 20 nm (Anodisk, Fisher Scientific) was used as the substrate for bead masking and SiO₂ deposition. The structure of this membrane is shown in Figure A.4.

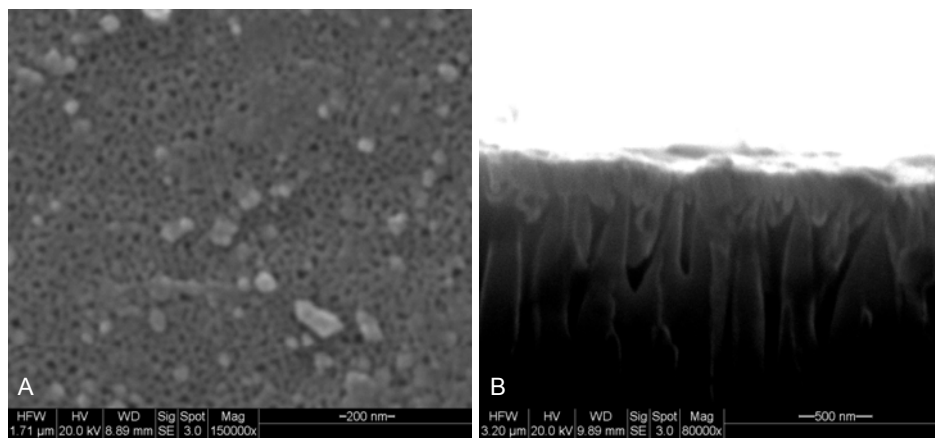


Figure A.4 Alumina membrane with 20 nm pore diameter. A, top view; B, cross-section.

The pores of this membrane have assymetrical geometry: 20 nm diameter on one side of the membrane (Figure A.4(A)), and 200 nm diameter on the other. In cross-section (Figure A.4(B)), the each 200 nm pore can be observed to branch into several smaller pores with 20 nm diameter at the surface. The branching region is 0.5 – 1 μ m in

thickness, with the rest of the pore (59 μm length) possessing a diameter of 200 nm. This morphology is particularly suited for the bead/ SiO_2 masking process since it allows synthesis of long 200 nm diameter nanowires while enabling the use of much thinner SiO_2 film to block the pores (Chapter 5). Furthermore, the 20 nm pores can themselves be used for template synthesis to generate nanostructures of the same size (Chapter 6).

The beads were deposited on the alumina surface with 20 nm pores as before, and SiO_2 sputtering was carried out under the following conditions: RF power of 350 W, stage RF bias of 40 W and stage temperature of 50° C for 20 minutes (Figure A.5(A)). The microbeads were removed by ultrasonication for 2 minutes, leaving open pores where the beads were previously located (Figure A.5(B)).

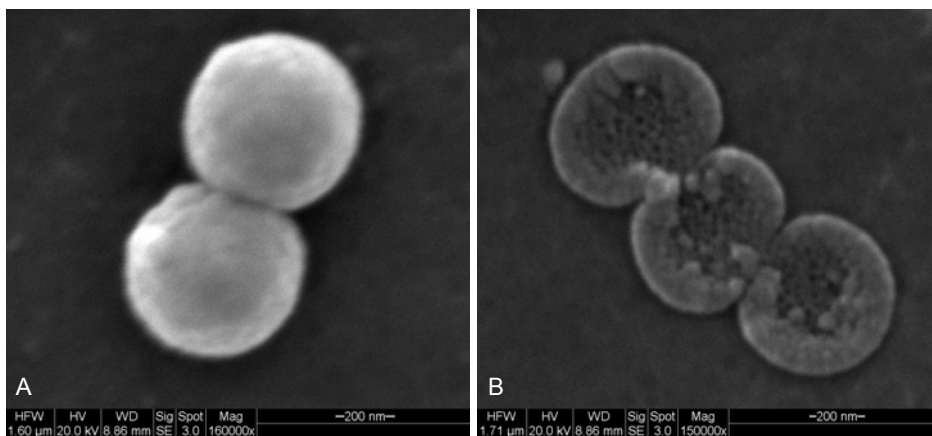


Figure A.5 Sputtered 50 nm SiO_2 film on alumina with 20 nm pore size. A, Microbeads after SiO_2 sputtering; B, SiO_2 after removal of microbeads with ultrasonication.

After the removal of the beads, the alumina samples were coated with a metal film which acted as a conductive seed layer for subsequent electroplating step. Ti was sputtered (Denton Sputtering system) first (200 W DC power on Ti target, rotating

sample stage, 35 sccm Ar flow, for 30 seconds), followed by Au (400 W, rotating sample stage, 35 sccm Ar flow, for 100 seconds). The samples were then electroplated with Au in a custom built electroplating bath at 58° C for 7 minutes at 10 mA of DC current. Since the sample holder for the electroplating setup is a simple alligator clip, the alumina membranes were first mounted on a glass slide with the Au-sputtered side up using the surface tension of a water droplet. This prevented the breaking of the alumina samples by pressure exerted by the sample mount clip. After the electroplating was complete, samples were rinsed with DI water, and allowed to air-dry. For fabrication of nanosensors, the sample was then mounted on a glass slide with Au-coated side down using conducting paint. Conducting paint was also used to form a contact pad and to connect it with the sample. The sample edges were then coated with thermal wax to protect the conducting paint from NaOH solution, which was used to dissolve the alumina (0.5 M NaOH, 40 minutes). After immersion in NaOH, sample edges were recoated with thermal wax to improve insulation and eliminate leakage currents. The samples were then ready for use as nano-electrodes for dopamine sensing, or electrode surface could be modified by coating with a thin o-PPy for improved selectivity (Chapter 6).

The dopamine detection was carried out with a 3 electrode electrochemical setup described in Chapter 2, using chronoamperometry, cyclic voltammetry, and stripping differential pulse voltammetry functions of the Gamry potentiostat mounted in a personal computer.